AN OPTICAL PHASE LOCKED LOOP
FOR SEMICONDUCTOR LASERS

by

Richard L. Boyd

S.M., Massachusetts Institute of Technology (1988)

SUBMITTED TO THE DEPARTMENT OF AERONAUTICS AND ASTRONAUTICS
IN PARTIAL FULFILLMENT OF THE REQUIREMENTS
FOR THE DEGREE OF

MASTER OF SCIENCE

at the

MASSACHUSETTS INSTITUTE OF TECHNOLOGY

May 1988

© Richard L. Boyd, 1988

Signature of Author _____ May 20, 1988
Department of Aeronautics and Astronautics

Certified by _____ 5/20/88
Dr. Shaoul Ezekiel
Thesis Supervisor

Certified by _____ 20 May 88
Daniel J. Fitzmartin
Company Supervisor

Accepted by _____
Professor Harold Y. Wachman
Chairman, Departmental Graduate Committee

AN OPTICAL PHASE LOCKED LOOP
FOR SEMICONDUCTOR LASERS

by

Richard L. Boyd

Submitted to the Department of Aeronautics and Astronautics
on May 18, 1988 in partial fulfillment of the
requirements for the Degree of Master of Science in
Aeronautics and Astronautics

ABSTRACT

        An optical phase locked loop was studied, designed, and partially
built and tested. The experiment used semiconductor laser diodes at
1300 nm, polarization preserving optical fibers and couplers, a Fabry-
Perot interferometer, and low frequency and wideband receivers. It was
confirmed that the white frequency noise of the lasers, as well as their
frequency modulation response, were critical factors in the phase locked
loop. In addition, a feedback loop involving a electro-optic phase
modulator and serrodyne frequency shifting was presented.

Thesis Supervisors: Dr. Shaoul Ezekiel
                      Professor of Aeronautics and Astronautics, and
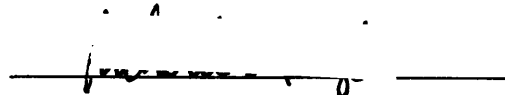   Electrical Engineering and Computer Science

                      Daniel J. Fitzmartin
                      Section Chief, The Charles Stark Draper
                      Laboratory, Inc.

ACKNOWLEDGMENT

I would like to thank Daniel Fitzmartin, my supervisor at Draper Laboratory, for his invaluable support and assistance in designing and implementing the PLL system; Seth Davis, my co-worker at CSDL, for his patience and time spent helping with the PLL experimental work; and The Charles Stark Draper Laboratory for providing the support for this research under IR&D project #237.

Publication of this report does not constitute approval by the Draper Laboratory of the finding or conclusions contained herein. It is published for the exchange and stimulation of ideas.

I hereby assign my copyright of this thesis the The Charles Stark Draper Laboratory, Inc., Cambridge, Massachusetts.

Richard L. Boyd

Permission is hereby granted by The Charles Stark Draper Laboratory, Inc., to the Massachusetts Institute of Technology to reproduce any or all of this thesis.

3

TABLE OF CONTENTS

LIST OF FIGURES

LIST OF FIGURES (Cont.)

CHAPTER 1

INTRODUCTION AND MOTIVATION

1.1   Motivation

Communication systems of the future will undoubtedly involve
fiber optics, since optical communications have intrinsically wide band-
widths, and offer increased security, electromagnetic interference
rejection, low loss, and lightweight cables. The first lightwave commu-
nication systems relied upon amplitude modulation for encoding the
signal on the optical carrier. For digital systems, this was analogous
to the telegraph systems of old: the light was just turned on and off
for ones and zeros. These systems used light emitting diodes or laser
diodes as light sources, and they worked well for this purpose. The
incoherence of the optical source is not critical in on-off keying and
direct detection. As with radio frequencies, though, it is more effi-
cient in terms of the received signal power required to achieve a given
bit error rate to use frequency or phase modulation, and thus coherent
detection, which requires that frequency or phase of the carrier be
known in the receiver in order to demodulate the signal. The basic
demodulation scheme is to multiply the transmitted signal with a local
oscillator whose frequency is fixed with respect to the carrier. The
result of this multiplication of two sinusoids is a difference phase
term (the sum term is filtered out). The data can then be recovered
from this difference term.

When the frequency difference between the carrier and the local
oscillator is zero, the receiver performs homodyne demodulation. This
is opposed to heterodyne demodulation, which uses nonzero frequency

difference. Homodyne receivers are more desirable because all of the electronics work at baseband, or the bandwidth of the data. This reduces both the complexity of the electronics. More importantly, the noise is 3 dB less than in the heterodyne case because no image noise is generated. The difficulty here is that when phase modulation is employed, the receiver has to track and match not just the frequency of the carrier, but also the phase. The scheme for phase locking to a signal is called a phase locked loop, or PLL for short.

Figure 1.1 shows a Costas loop, a scheme for homodyne demodulation of biphase modulation. This is a type of phase modulation for digital transmission. The phase of the carrier is either zero or 180 degrees, which corresponds to plus or minus one times the carrier (see Figure 1.2). One half of the loop mixes the transmitted signal with the local oscillator and outputs the demodulated data. The other half of the loop mixes the same two signals, but with a 90 degree phase shift introduced in the local oscillator signal. The resulting signal is then multiplied by the recovered data from the first half, which for biphase modulation strips off the data. This signal is then fed back to the local oscillator. The feedback loop is designed to force the local oscillator to track the phase of the carrier. This part of the Costas loop is the phase locked loop.

1.2   Thesis Objective

As alluded to earlier, LEDs are not good light sources for coherent communications because their spectral linewidths are much greater than the bandwidth of the data, typically hundreds of gigahertz wide. The solution is to use single mode laser diodes, which have much narrower linewidths. Since the instantaneous frequency of the laser diodes does not vary greatly from the center frequency, it is possible to track an optical carrier frequency with another laser diode.

The purpose of this project is to study the problems involved in designing and building an optical phase locked loop. An actual system was built which demonstrated many of the important issues. The system
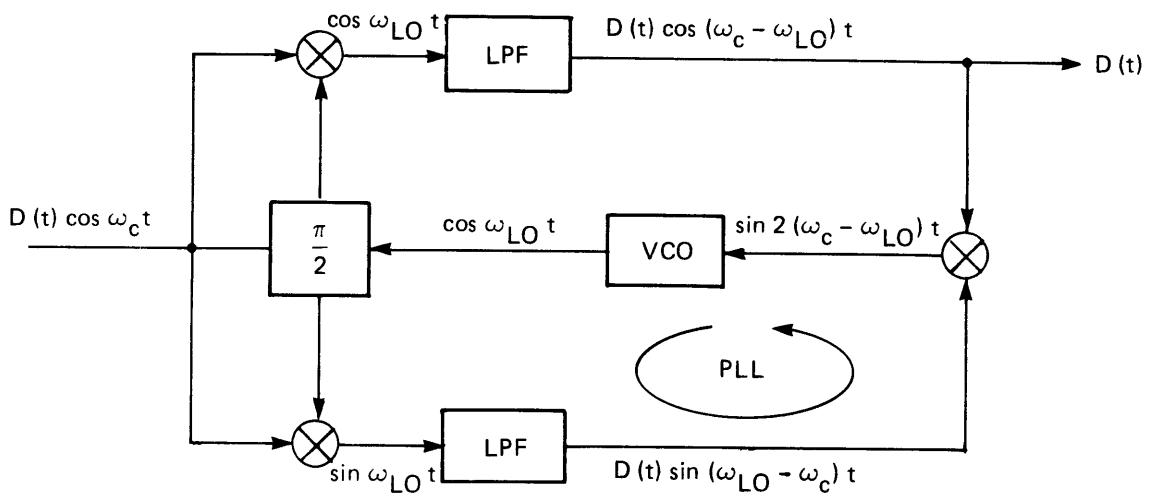
Figure 1.1. Costas loop.

$$y(t) = \sin\left(\omega_c t + D(t)\,\frac{\pi}{2}\right)$$
$$= D(t)\,\text{soc}\,(\omega_c t)$$
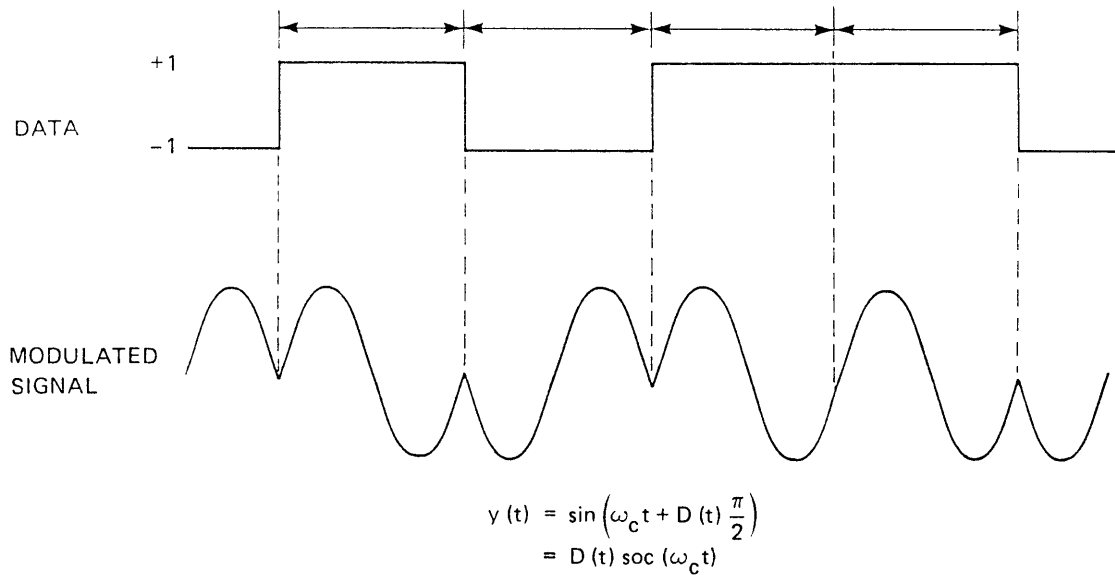
Figure 1.2. Biphase modulation.

10

attempted to phase lock two semiconductor lasers using electrical feed-
back in the absence of any data modulation. This is the first step in
realizing a homodyne communication system for lightwave communications.

1.3   Outline of Report

Chapter 2 of this report contains a discussion of control theory
and stochastic analysis as they pertain to the phase locked loop.
Chapter 3 describes the components that make up the experimental system.
In Chapter 4, several tests and data measurements are explained, and the
limitations of the system are identified. Chapter 5 describes how work
would continue with a new system and components. Finally, Chapter 6
summarizes the conclusions and presents some additional recommendations
for further work in the area.

CHAPTER 2

BASIC PHASE LOCKED LOOP - CONTROL THEORY

2.1   Classical Electrical PLL Block Diagram and Explanation

Figure 2.1 shows a block diagram of a classical phase locked loop. The signal y(t) is the unmodulated carrier to which the local oscillator signal x(t) will be locked. The phase detector puts out a signal e(t) proportional to the phase difference between x(t) and y(t). This signal is then filtered by some sort of low pass filter and then sent to the voltage controlled oscillator (VCO). The VCO outputs a signal whose frequency is proportional to the input voltage. This output is x(t), and is phase locked to the input y(t).

The PLL can best be understood by imagining that the signals x(t) and y(t) are initially phase locked, that is their frequencies and phases are exactly the same. In this case, the error signal e(t) is zero, and the filter output is whatever is necessary to match the frequencies. Now imagine that y(t) takes a step in phase, so that e(t) becomes positive. The VCO is therefore driven to a higher frequency, and x(t) begins to advance in phase with respect to y(t) since its frequency is higher. As this phase increases, though, e(t) will decrease as the phase of x(t) approaches the phase of y(t). This will, in turn, force the VCO to put out a gradually lower frequency, until e(t) is nulled again. Thus the loop will force x(t) to stay phase locked to y(t).
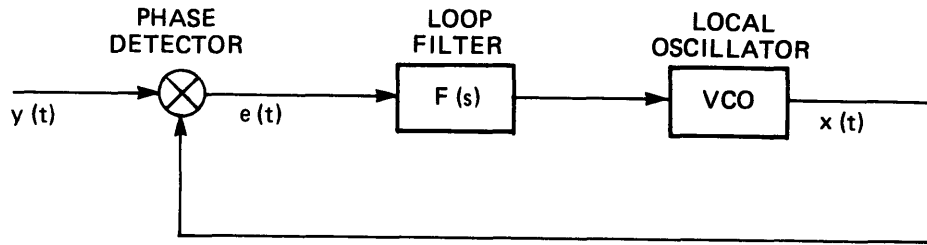
Figure 2.1. PLL block diagram.

2.2 Control Theory - Transfer Functions

Figure 2.2 shows the PLL block diagram in terms of control theory. The signals are now considered to be the phases of x(t) and y(t). The phase detector is therefore just a subtraction block, creating e(t) = y(t) - x(t). The loop filter is

$$\frac{K_a(s + \omega_1)}{s} \tag{1}$$

This will create a type 2 system (see Section 2.4). The VCO is now a perfect integrator with gain K_b, represented by K_b/s. Thus, for a constant input, the VCO outputs a frequency, which in turn is just a ramp in phase.
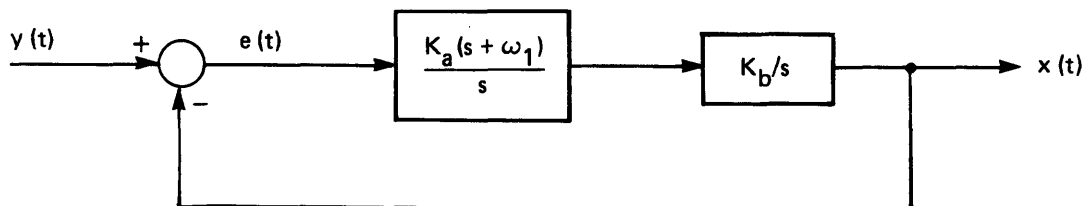
Figure 2.2. PLL block diagram - control theory.

2.3 G(s) : Forward Transfer Function

The blocks combine in series to form a forward transfer function

$$G(s) = \frac{X(s)}{Y(s)} = \frac{K(s + \omega_1)}{s^2} \tag{2}$$

13

where

$$K = K_a K_b$$

Figure 2.3 shows the bode plot of G(s). For stability, the crossover
frequency of the magnitude must occur before the phase crosses through
180 degrees. The zero at ω_1 causes the phase to be -90 degrees for fre-
quencies well above ω_1. The gain K controls the crossover point by
shifting the magnitude graph up or down. In this case, the loop will be
stable for any value of gain, but for a safe phase margin, the crossover
frequency should be above ω_1. For crossover frequencies greater than
about three times the loop gain K equals the crossover frequency. In
reality, though, high frequency rolloff of actual components and nonzero
time delay around the feedback loop will cause the phase the drop below
-180 degrees at higher frequencies. The time delay of a signal travell-
ing around the loop merely adds a linear phase to the transfer function.
This phase increases linearly with frequency, and is:

$$\phi_{delay} = (2 \pi f)(\text{time delay}) \tag{3}$$

For instance, for a delay of 5 ns (1 meter of electrical length), the
additional phase delay is 90 degrees at 50 MHz. Thus, a crossover fre-
quency above 50 MHz would cause the system to be unstable.

2.4   H(s) and E(s) - Closed Loop Transfer Functions

The next step in analyzing the feedback loop is to examine the
responses due to various deterministic inputs. For this, the closed
loop error transfer function is used.

$$
\begin{aligned}
e(t) &= y(t) - x(t) \\
E(s) &= Y(s) - X(s) \\
&= Y(s)*(1 - X(s)/Y(s)) \\
&= Y(s) \ \frac{1}{1 + G(s)} \\
&= Y(s) \ \frac{s^2}{s^2 + Ks + K\omega_1} \tag{4}
\end{aligned}
$$

14
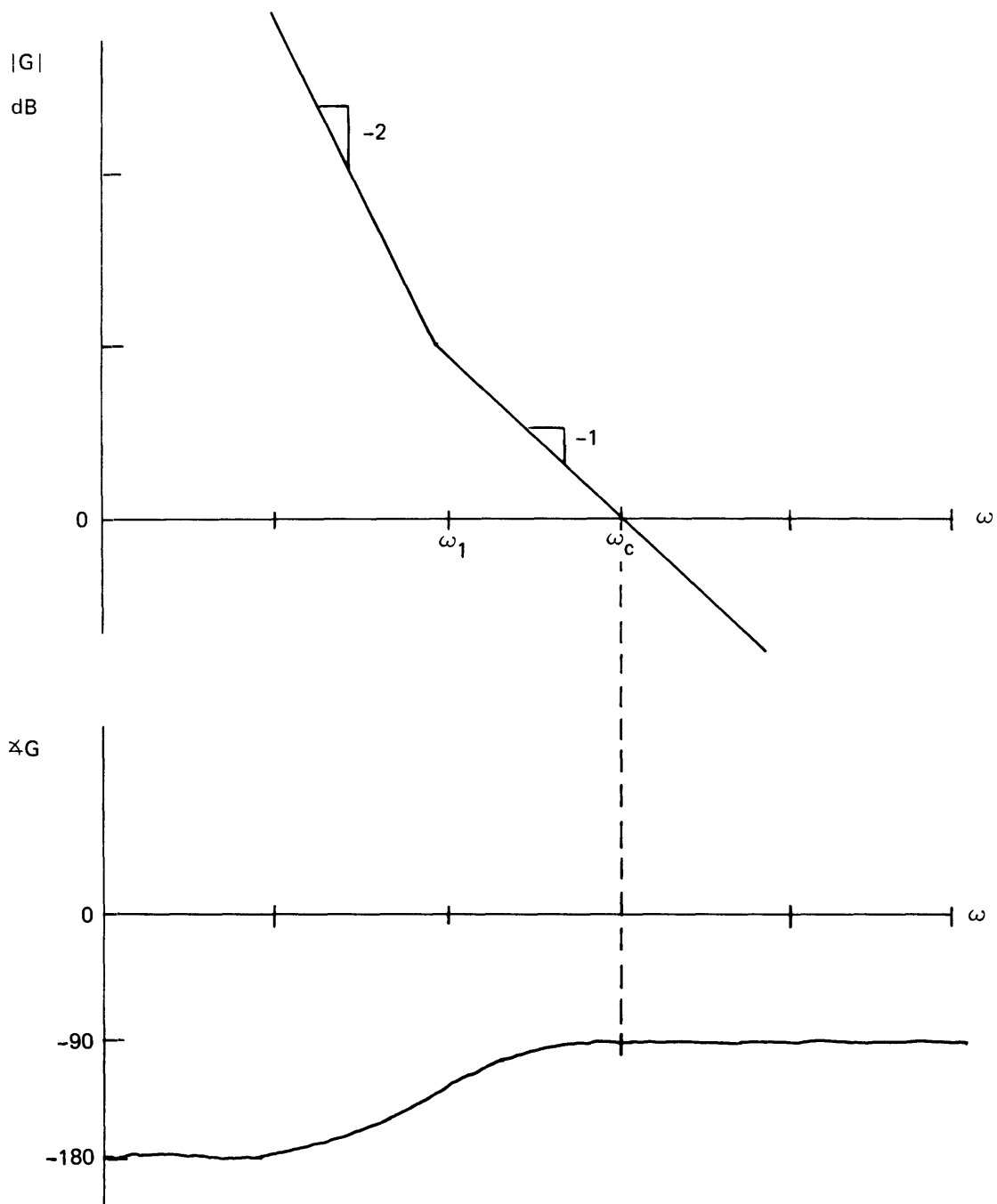
Figure 2.3. Bode plot of G(s).

The steady state errors can then be found by applying Equation (5), the final value theorem for Laplace transforms.

$$e(t - \text{infinity}) = \lim_{s \to 0} sE(s) \qquad (5)$$

These steady state errors for three important input signals are summarized in Figure 2.4. This system is considered a type 2 system because of the s^2 in the denominator of G(s). The importance of a type 2 system is that it has zero steady state error for both step and ramp inputs. This is necessary in a phase locked loop because a ramp in phase is the same as a step in frequency, and the loop needs to be able to track the frequency. Also, the loop tracks linear frequency variations, or phase parabolas. The final, or average, value of the phase error for a frequency ramp is shown in the figure. Thus, for large K, the loop will have a very small, but not zero, phase error due to frequency shifts.

INPUT	Y (s)	$\lim_{s \to 0} sE(s)$
STEP	$\frac{1}{s}$	0
RAMP	$\frac{1}{s^2}$	0
PARABOLA	$\frac{1}{s^3}$	$\frac{1}{K\omega_1}$

Figure 2.4. Steady state errors.

2.5 Time Dependent Error

The denominator of E(s) is important in determining the natural frequency and damping of the loop. If E(s) is rewritten

16

$$E(s) = Y(s) \frac{s^2}{s^2 + 2\zeta\omega_n s + \omega_n^2} \qquad (6)$$

ω_n is the natural frequency of the loop and ζ is the damping ratio. The meaning of these two parameters is seen in the step error response. Instead of looking at the steady state value, consider the time response. This is easily found by inverse transforming E(s) for a step input.

$$e(t) = \begin{cases} e^{-\zeta\omega_n t} \left[\cosh\left(\omega_n \sqrt{\zeta^2-1}\ t\right) - \frac{\zeta}{\sqrt{\zeta^2-1}} \sinh\left(\omega_n \sqrt{\zeta^2-1}\ t\right)\right], & \zeta > 1 \\ e^{-\zeta\omega_n t} (1 - \omega_n t) & , \zeta = 1 \\ e^{-\zeta\omega_n t} \left[\cosh\left(\omega_n \sqrt{1-\zeta^2}\ t\right) - \frac{\zeta}{\sqrt{1-\zeta^2}} \sinh\left(\omega_n \sqrt{1-\zeta^2}\ t\right)\right], & \zeta < 1 \end{cases}$$

Figure 2.5 shows the response for several values of ζ. Clearly, ζ determines the amount of overshoot, if any, of the response. The natural frequency and ζ together determine how quickly the system responds: a
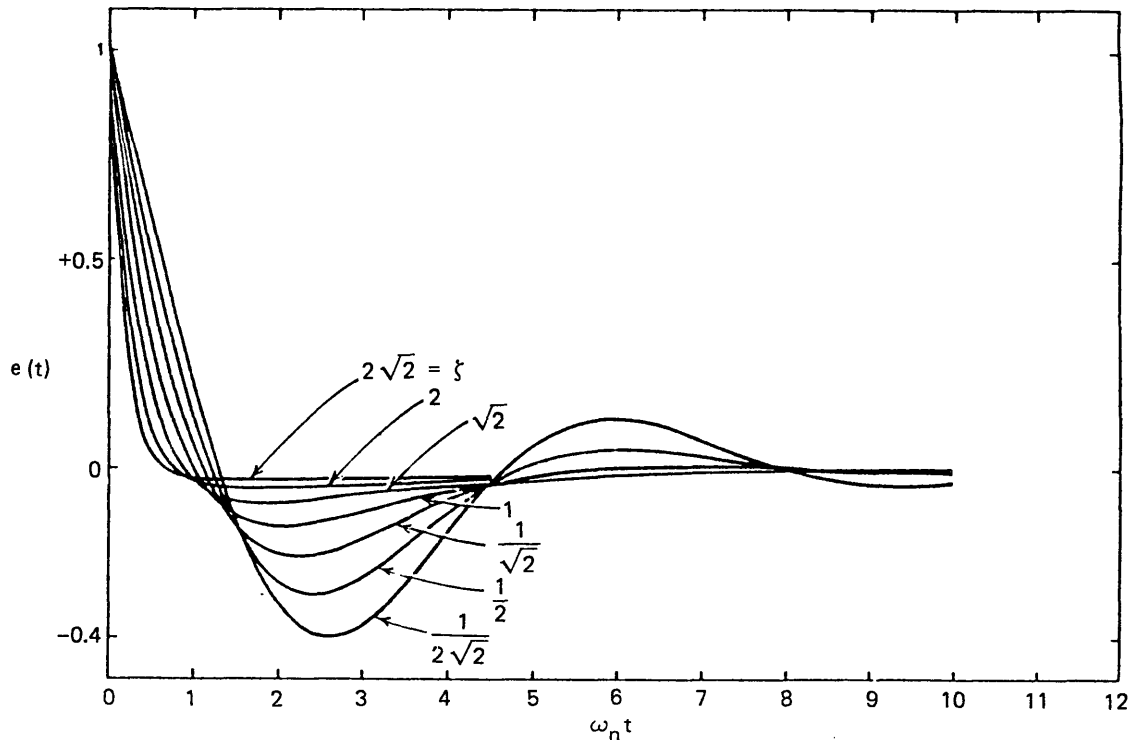

Figure 2.5. Step response of PLL (from Reference 3).

17

higher ω_n will cause a faster response. A good compromise between over-
shoot and response time is $\zeta = 0.707$, but higher values are certainly
acceptable.

2.6   Pull-In Range and Acquisition

Until now, the analysis has assumed that the PLL was initially
locked. In reality, though, there will be some frequency difference
between the LO and the carrier when the loop is first turned on. By
analyzing the nonlinear differential equations which describe the
unlocked feedback loop, Blanchard [Ref. 3] has shown that any second
order PLL will eventually lock for any initial frequency difference.
The time for such acquisition is

$$T_{acq} = \frac{\Omega_0^2}{2\zeta\omega_n^3}$$

where Ω_0 is the initial frequency error

This assumes, though, that the loop is exactly described by the
second order model. In the present case, the loop cannot be considered
properly modelled for frequencies larger than the G(s) crossover fre-
quency, mainly because of the time delay described earlier. For this
reason, the loop probably will not be able to acquire phase lock if the
initial difference frequency is much greater than the crossover fre-
quency. The solution to this problem is to force the LO frequency to
increase or decrease until the loop can lock on its own. This frequency
sweep must be slower than $1/K\omega_1$ (see Figure 2.4), or else the loop will
be unable to acquire lock.

2.7   Noises - RMS Values

The final and most important aspect of the analysis is the de-
termination of the RMS phase error. In the physical system, there will
be various noise sources that prevent the loop from exactly tracking the
input phase at every instant. The steady state analysis showed that on

18

average the tracking will be almost exact, but in reality the square of
the phase error will have a distribution as shown in Figure 2.6. Since
most of the noise sources are considered to be white noise, the curve is
approximately gaussian, described by Equation (7).

$$f(x) \quad = \quad \frac{1}{\sqrt{2\pi}\ \sigma} \ e \ \frac{-x^2}{2\sigma^2} \tag{7}$$

x/σ	$\int_{-x}^{x} f(x)\, dx$
0	0
0.5	0.38
1	0.68
1.5	0.87
2	0.95
2.5	0.988
3	0.997
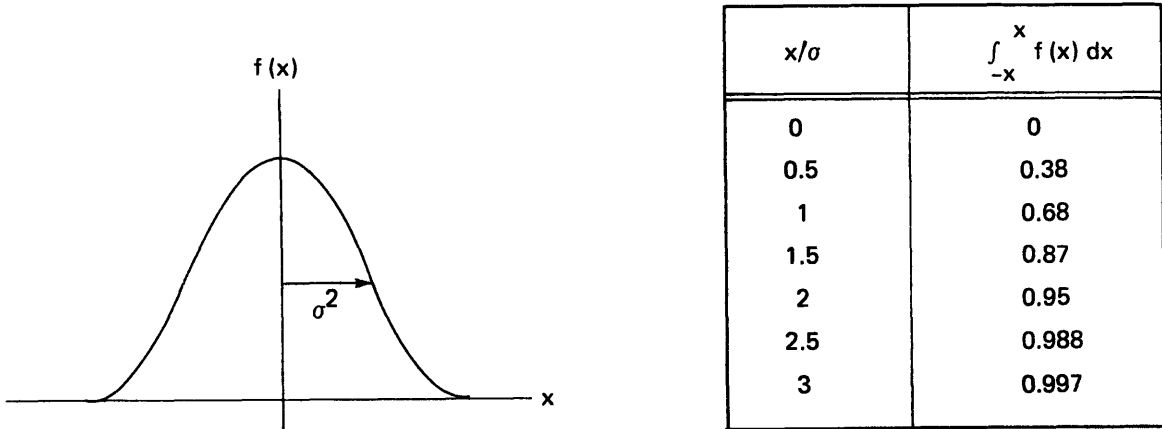
Figure 2.6. Gaussian distribution.

The probability of the phase error being within some range is determined
by the area under the curve in that range. The distribution is charac-
terized by its variance, σ, which is determined by the loop transfer
functions. Figure 2.6 also lists the probabilities for several values
of x. As seen in the figure, the probability of the phase error being
within 3σ is 0.997. For the PLL, if the variance is 0.01 rad^2, then
there will be a 0.997 probability that the phase error will be less than
0.3 rad (about 17 degrees). This is a reasonable if somewhat optimistic
number for phase lock. A variance of 0.1 rad^2 leads to the phase error
being within 1 rad of zero. The phase detectors to be used in the
experiment actually have sinusiodal characteristics,

$$signal \quad = \quad sin(phase\ error)$$

19

This will result in a phase error signal which is not exactly proportional to the phase error. At phase error = 1 rad, however, sin(1 rad) = 0.84, and thus it can still be considered approximately proportional.

The actual variance of the system is determined through stochastic analysis. First the noise sources are included in the block diagram as in Figure 2.7. Essentially, each component will have noise associated with it, and it is also necessary to include the system response to a noisy input signal y(t). The sources are considered to be statistically independent, so the principle of superposition can be used to find the transfer function relating each source to the error signal.

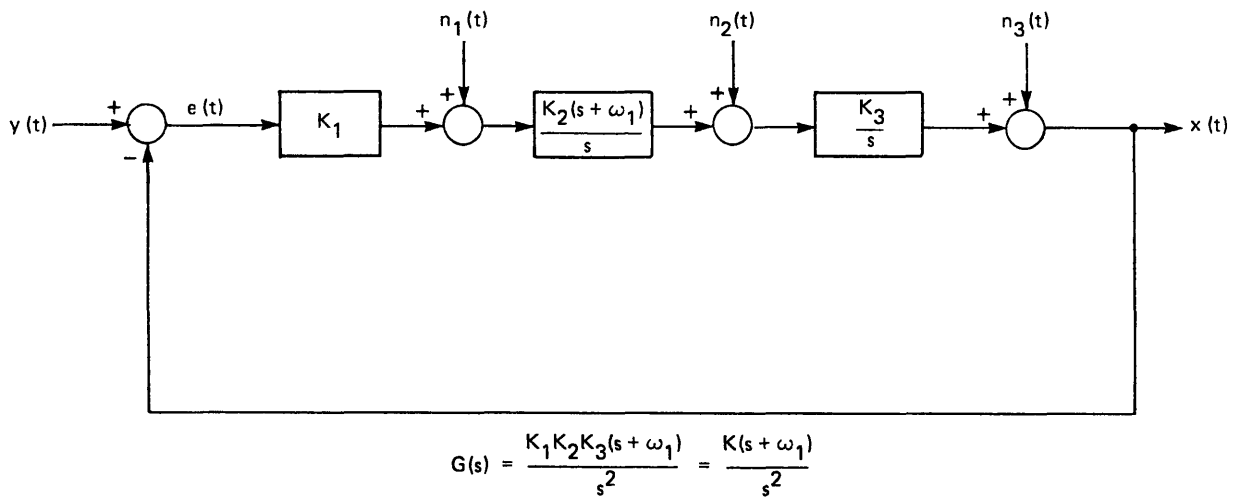$$G(s) = \frac{K_1 K_2 K_3 (s + \omega_1)}{s^2} = \frac{K(s + \omega_1)}{s^2}$$

Figure 2.7. PLL block diagram including noise sources.

Equations (8a) through (8d) show these relations:

$$\frac{E(s)}{N_1(s)} = \frac{1}{K_1} \frac{K(s + \omega_1)}{s^2 + Ks + K\omega_1} \tag{8a}$$

$$\frac{E(s)}{N_2(s)} = \frac{1}{K_1 K_2} \frac{Ks}{s^2 + Ks + K\omega_1} \tag{8b}$$

20

$$\frac{E(s)}{N_3(s)} = \frac{s^2}{s^2 + Ks + K\omega_1} \tag{8c}$$

$$\frac{E(s)}{Y(s)} = \frac{s^2}{s^2 + Ks + K\omega_1} \tag{8d}$$

The expected squared value, or variance, of the phase error is then given by Equation (9):

$$\sigma^2 = \overline{e^2} = \frac{1}{2\pi j} \int_{-j\infty}^{+j\infty} S(s)|F(s)|^2 ds \tag{9}$$

where $S(s)$ is the two-sided spectral density of the noise, and $F(s)$ is the corresponding transfer function for the noise.

The noises $n_1(t)$ and $n_2(t)$ will be white, characterized by a constant spectral density, N_i. The noise on the input, as well as $n_3(t)$ will be white frequency noise, which converts to a N_{ia}/s^2 phase noise spectrum, and a statistically independent 1/f frequency noise term, which converts to a $|N_{ib}/s^3|$ phase noise spectrum. Equations (10a) through (10d) show the results from applying Equation (9) for each noise source.

$$\sigma_1^2 = \frac{N_1}{K_1^2} \left(\frac{K+1}{2}\right) \approx \frac{K}{2K_1^2} N_1 \tag{10a}$$

$$\sigma_2^2 = \frac{K}{2(K_1K_2)^2} N_2 \tag{10b}$$

$$\sigma_3^2 = \frac{1}{2K} N_{3a} + \frac{\pi}{K^2} N_{3b} \tag{10c}$$

$$\sigma_y^2 = \frac{1}{2K} N_{ya} + \frac{\pi}{2K^2} N_{yb} \tag{10d}$$

Appendix A shows the derivation of these expressions. Finally, the total variance is:

$$\sigma^2 = \frac{\pi}{2K^2}(N_{yb} + N_{3b}) + \frac{1}{2K}(N_{ya} + N_{3a}) + \frac{K}{2}\left(\frac{N_1}{K_1^2} + \frac{N_2}{K_1^2 K_2^2}\right) \qquad (11)$$

This equation shows that increasing the loop gain K, which is also the open loop crossover frequency, will decrease the noise from some sources while increasing the noise from others.

CHAPTER 3

OPTICAL PLL - COMPONENTS

3.1   Block Diagram

        This chapter describes most of the components that make up the
optical phase locked loop. Figure 3.1 is a block diagram that includes
all of the physical components of the system. The transmitter laser
provides the source to which the local laser will be locked. Polariza-
tion maintaining optical fibers connect the optical components, and are
shown in the figure as double lines. The optical coupler combines the
optical signals, and the detectors convert the light into electrical
signals. Finally, the detectors serve as the phase detectors in the
PLL.

3.2   Lasers and Drive Circuitry

        The lasers used in the PLL are Toshiba DFB semiconductor laser
diodes at wavelengths near 1300 nm. Their light producing qualities are
examined in Chapter 4. Electrically, the devices are merely diodes. By
controlling the forward current and temperature of the laser diode, the
output power, lasing frequency, and noise statistics can be controlled.

        Figure 3.2 shows a simplified circuit that controlled the laser
diodes. A set of batteries and a potentiometer provided an adjustable
bias current for the laser. Figure 3.3 shows the output power depen-
dence on current, and indicates a minimum, or threshold, current of
around 30 mA. The potentiometer allowed the current to be adjusted from
around 50 mA to around 100 mA. The bias current was measured by an in-
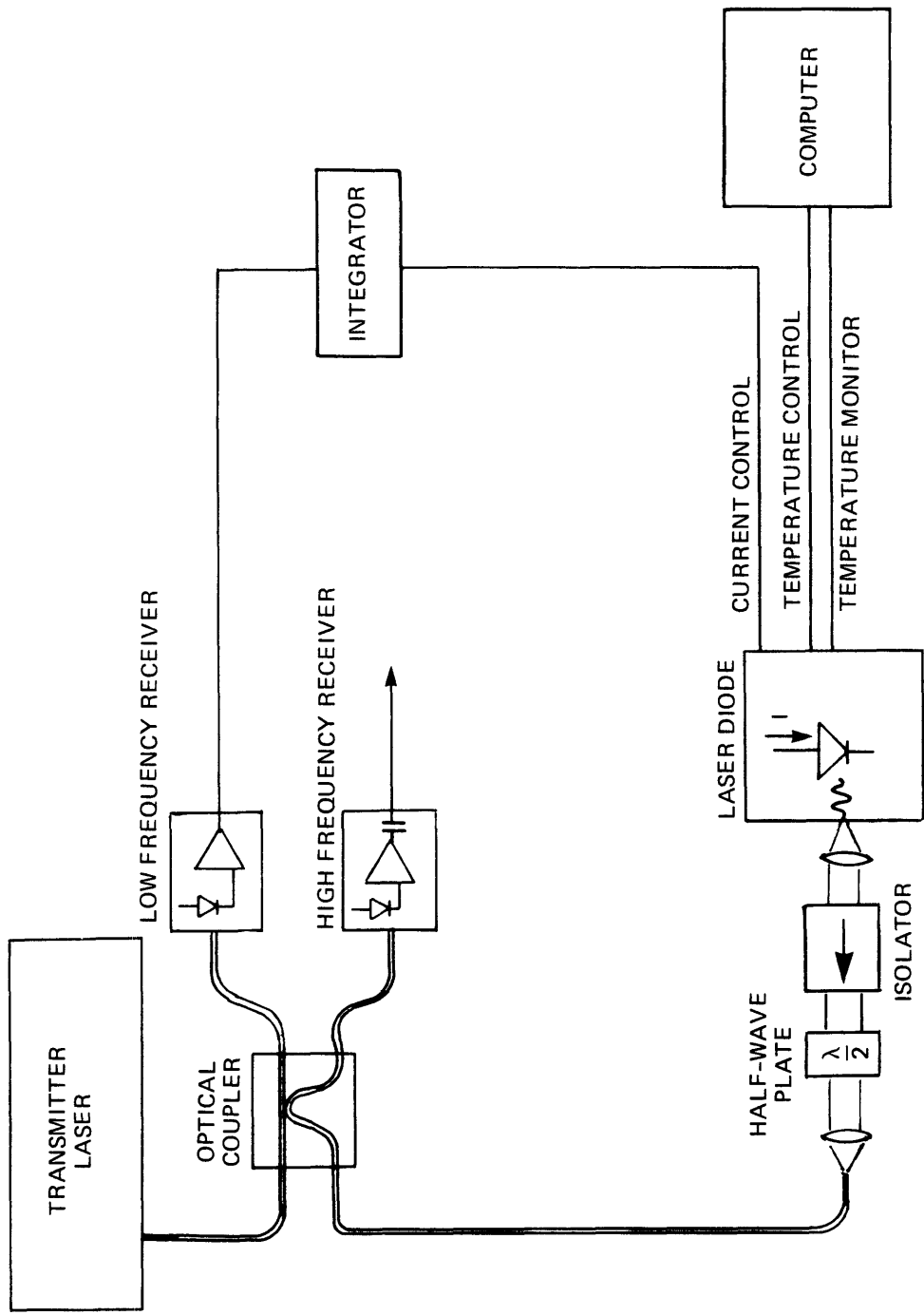line ammeter.
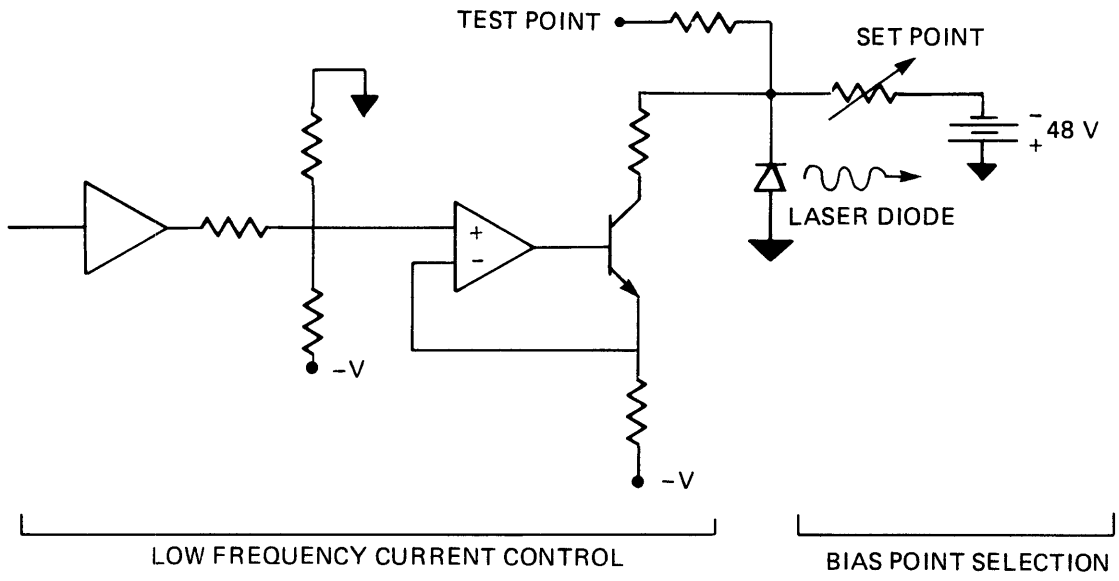
Figure 3.1. PLL component block diagram.
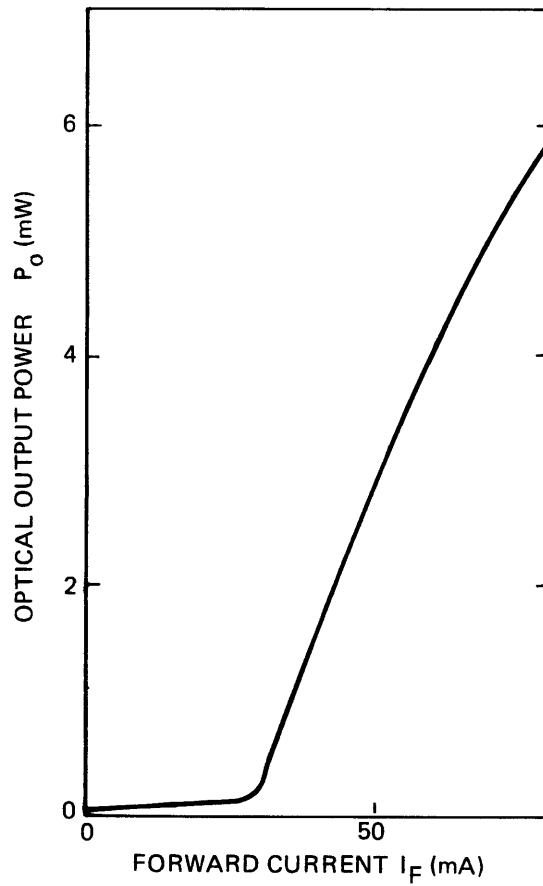
Figure 3.2. Current control circuit.

Figure 3.3. Power vs. injection current.

The low-frequency current control allowed an additional zero to ten mA to be added to the bias current. It consisted of a voltage controlled current source with a transfer constant of 0.5 mA/V. A test point in the circuit allowed the current source to be tested, and its response was flat at to 100 kHz.

An additional section of the laser drive circuit, that was not used in this experiment, was a high fequency current source. This source allowed the laser current to be controlled from 10 kHz to near 500 MHz. The two current sources, then, would allow the current to be controlled in the DC to 500 MHz frequency band.

The entire laser circuit was enclosed in a temperature controlled environment. The temperature was held to a $10^{-5} °C/s$ drift by a temperature control loop which used thermistors and thermoelectric coolers. This degree of control was necessary due to the sensitivity of the laser to temperature, as discussed in Chapter 4. The set point of the temperature control loop was adjustable by a control voltage, which was selectable through a computer controlled digital-to-analog converter.

3.3. Optical Components, Fiber, Polarization, Coupler

The light exits the laser diode in a diverging cone that is collimated by a lens placed close to the laser. The light is then sent through an optical isolator, which linearly polarizes it, and only allows light to pass in one direction. Figure 3.4 shows how the isolator works. The first polarizer linearly polarizes the light. Next, the Faraday rotator rotates this linear polarization by 45 degrees clockwise. The output polarizer is aligned to allow all the light to pass. Any light reflected back toward the isolator from anywhere in the system then undergoes the reverse process. The output polarizer allows only a certain polarization to pass. The faraday rotator then rotates the light clockwise by 45 degrees clockwise, but since the light is travelling in the opposite direction, it meets the input polarizer oriented in exactly the wrong direction. Thus the light will not pass through the
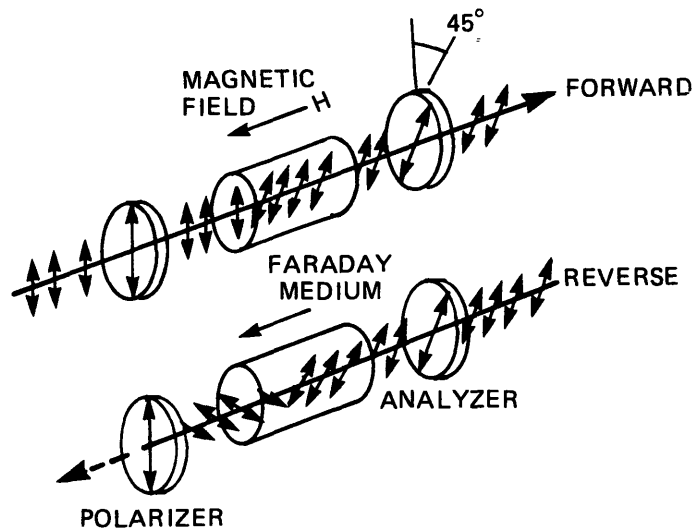
26

Figure 3.4. Optical isolator.

input polarizer and interact with the laser. With real polarizers,
though, the isolation is not perfect, and in this case is on the order
of 30 dB. In general this is not enough since very little optical feed-
back is sufficient to disrupt the coherence of the laser. Further iso-
lation is obtained by tilting optical faces wherever possible and using
antireflection coated surfaces.

In the optical path after the isolator is a half-wave plate.
This device is capable of rotating linearly polarized light to any
orientation. It works on the principle of birefringence. Birefringence
occurs in a substance when the index of refraction is different for dif-
ferent polarizations of light. The effect is to have light travelling
through the substance at different speeds for different polarizations
(see Figure 3.5). The half-wave plate is made of such a substance whose
length is precisely controlled to cause light polarized on one axis to
be delayed by 180 degrees with respect to the other axis. By orienting
the linearly polarized light at some angle with respect to these axes,
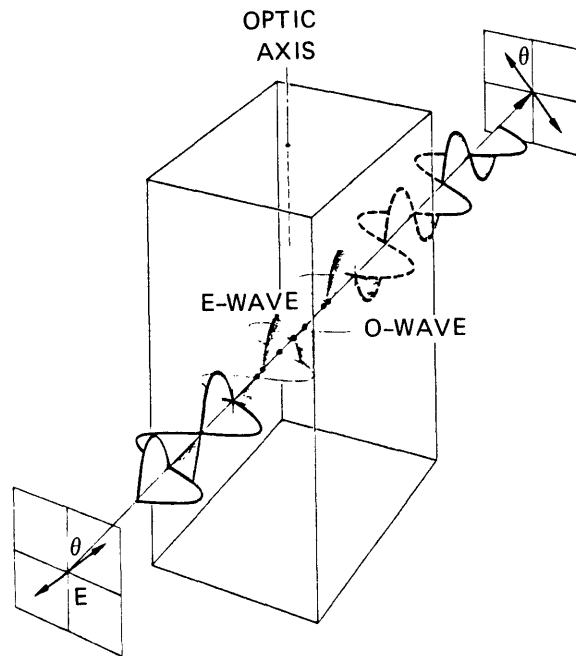it will emerge linearly polarized, but with a different orientation.

Figure 3.5. Half-wave plate.

Light emerges from the polarizer and is focused down to a point by a lens. The point coincides with the end of an optical fiber, and thus the light is launched into the fiber. Once inside, the light maintains its linear polarization due to the makeup of the fiber. The polarization is important when the optical signals pass through the phase modulator and also when they are summed.

The optical coupler adds the two input optical signals and outputs the sum at the two outputs. The light is a travelling elec-tromagnetic wave which can be described by the time varying function

$$E(t) = \sqrt{P} \sin(\omega t + \phi)$$

where P is the optical power in watts, ω is the frequency of the light and ϕ is the phase. The lasers used had a wavelength of about 1289 nm (infrared), which makes $\omega = 2\pi f = 2\pi c/\lambda = 3.7 \times 10^{13}$ rad/s. The power gets split evenly between the two output ports, resulting in the the signals

$$E_{1,out} = \sqrt{\frac{P_1}{2}} \sin(\omega_1 t + \phi_1) + \sqrt{\frac{P_2}{2}} \sin(\omega_2 t + \phi_2) \qquad (12a)$$

$$E_{2,out} = \sqrt{\frac{P_1}{2}} \sin(\omega_1 t + \phi_1) - \sqrt{\frac{P_2}{2}} \sin(\omega_2 t + \phi_2) \qquad (12b)$$

Of course, this assumes that the light waves are lined up in space, which requires that they be linearly polarized with the same orientation. As mentioned before, the fiber used in this experiment is capable of maintaining the desired polarization.

3.4   Phase Detector

The optical receivers are relatively straightforward devices. They consist of a photodetector, and an avalanche photodiode which drives a transimpedence amplifier, as in Figure 3.6. The photodetectors act as square law detectors, converting light power into electrical current. Equation (13) describes this conversion.

$$i = R \, E_{light}^2 \qquad (13)$$

where R is the responsivity of the diode, measured in A/W.

Using the expression for the light signals coming from the coupler,

$$\frac{i}{R} = \frac{P_1}{2} \sin^2(\omega_1 t + \phi_1) + \frac{P_2}{2} \sin^2(\omega_2 t + \phi_2) + \sqrt{P_1 P_2} \sin(\omega_1 t + \phi_1) \sin(\omega_2 t + \phi_2)$$

$$= \frac{P_1}{4} [1 - \cos(2\omega_1 t + 2\phi_1)] + \frac{P_2}{4} [1 - \cos(2\omega_2 t + 2\phi_2)]$$

$$+ \frac{1}{2} \sqrt{P_1 P_2} [\cos((\omega_1 + \omega_2)t + (\phi_1 + \phi_2)) - \cos((\omega_1 - \omega_2)t + (\phi_1 - \phi_2))]$$

$$(14a)$$

Since the sum of the frequencies is around 1.5×10^{14} Hz, these terms are zero in an electrical realization, leaving

$$\frac{i}{R} = \frac{P_1}{4} + \frac{P_2}{4} + \frac{1}{2} P_1 P_2 \cos((\omega_1 - \omega_2)t + (\phi_1 - \phi_2)) \qquad (14.b)$$

The amplifier then converts this current into a voltage.
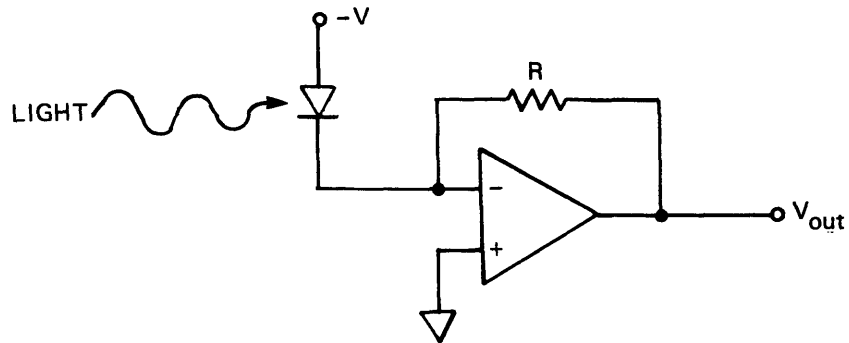

Figure 3.6. Optical receiver.

The two types of receivers used in the experiment cover the spectrum from DC to 200 kHz, and 10 kHz to 1 GHz. For the low frequency detector, the electrical output is 5×10^5 V/W, while the high-frequency receiver outputs 1 millivolt across 50 Ω for each microwatt of optical power.

The receivers also exhibit two types of noise. The thermal noise is due to random electron motions within the components, and is a band-limited white noise. It is measured by examining the output of the receiver on a spectrum analyzer with no light incident upon the detector. Values for the thermal noise are

Low frequency:
$$S_{th}(s) = -118 \text{ dBm} \quad (1 \text{ Hz})$$

High frequency:
$$S_{th}(s) = 137 \text{ dBm} \quad (1 \text{ Hz})$$

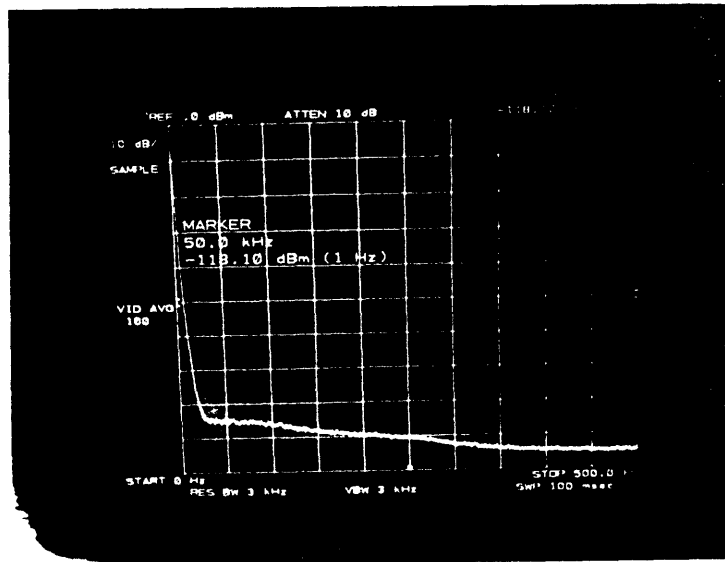as seen in the photos in Figure 3.7.
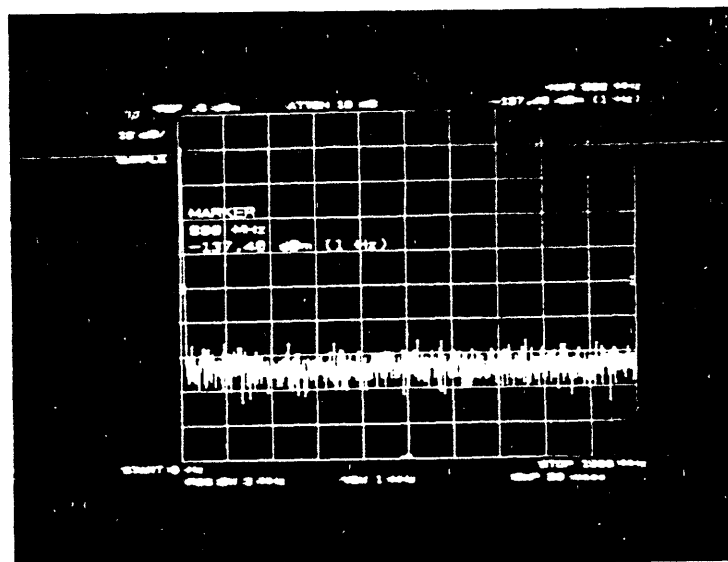
Figure 3.7a.   Low frequency receiver noise.

Figure 3.7b.   High frequency receiver noise.

The other noise is shot noise, which comes from the discrete nature of light. The photons which hit the photodetector each cause a current spike, as illustrated in Figure 3.8. The current will therefore have an average value dependent upon the number of photons (light power), around which the current varies. The variation is the shot noise, and theoretically should be

$$S_{shot}(s) = 2qKP \qquad (15)$$

where q is an electron charge, K is the receiver gain, and P is the light power. A measurement of this noise is made by shining a known light power on the receiver and examining the noise at the output. In this case, the shot noise is

$$S_{shot}(s) \leq -137 \text{ dBm} \quad (1 \text{ Hz})$$
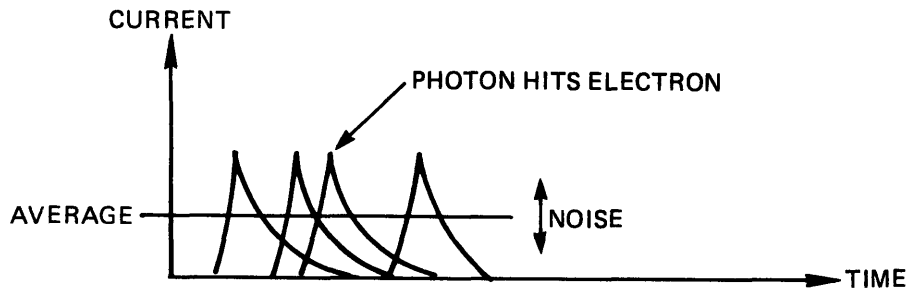
Figure 3.8. Shot noise.

3.5   Amplifiers and Filters

In the two paths between the low frequency receiver and the laser are integrators. A circuit plan for the low frequency integrator uses an op-amp, a resistor, and a capacitor, as shown in Figure 3.9. The transfer function of the filter is

$$F_1(s) = \frac{1}{sRC} \qquad (16)$$

Thus, the gain is 1/RC, and the circuit is an integrator.

$$\frac{V_o(s)}{V_i(s)} = \frac{1}{sRC}$$

Figure 3.9. Low-frequency integrator.

CHAPTER 4

EXPERIMENTAL RESULTS

4.1   Experimental Apparatus

Figures 4.1 through 4.5 are photographs of the experimental appa-
ratus. Figure 4.1 shows the launch system. The components, from left
to right, are the laser and lens in the temperature controlled box, the
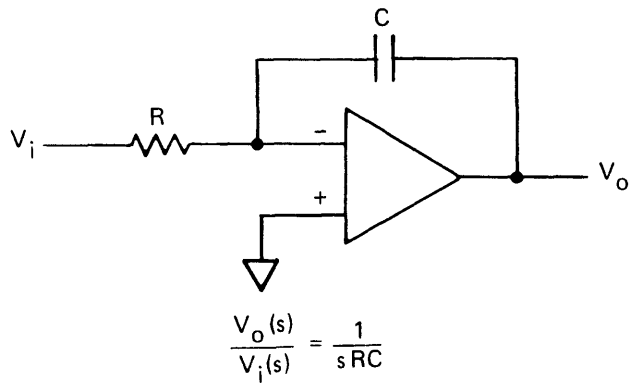isolator, the half-wave plate, and the lens and fiber. Figure 4.2
shows the launch system, a coupler, and the Fabry-Perot interferometer.
Figure 4.3 shows the high and low frequency receivers, an optical power
meter, and the compensation circuit. Figure 4.4 shows the entire setup
with both lasers. Finally, Figure 4.5 is a closeup of the laser drive
circuit. The laser itself is on the other side of the board.

4.2   Semiconductor Lasers

The lasers used in the PLL are Toshiba DFB semiconductor laser
diodes. Their advantages are the small size, mechanical ruggedness,
and small electrical power requirements as opposed to gas lasers, and a
simple modulation technique. These diode lasers, however, have two dis-
advantages. First, they typically have much broader spectral
linewidths than gas lasers. A gas laser, for instance, might have a
full width half maximum (FWHM) linewidth of 1 kHz, while a DFB laser
diode has a FWHM of 30 MHz. This wide linewidth manifests itself as
white frequency noise, and therefore introduces phase noise that the PLL
must take care of. The other main disadvantage of present laser diodes
is a 180° phase shift in the frequency response, as explained below.
Because of their size, and potential power, cost advantages, though,
laser diodes are the light source of choice for optical communication
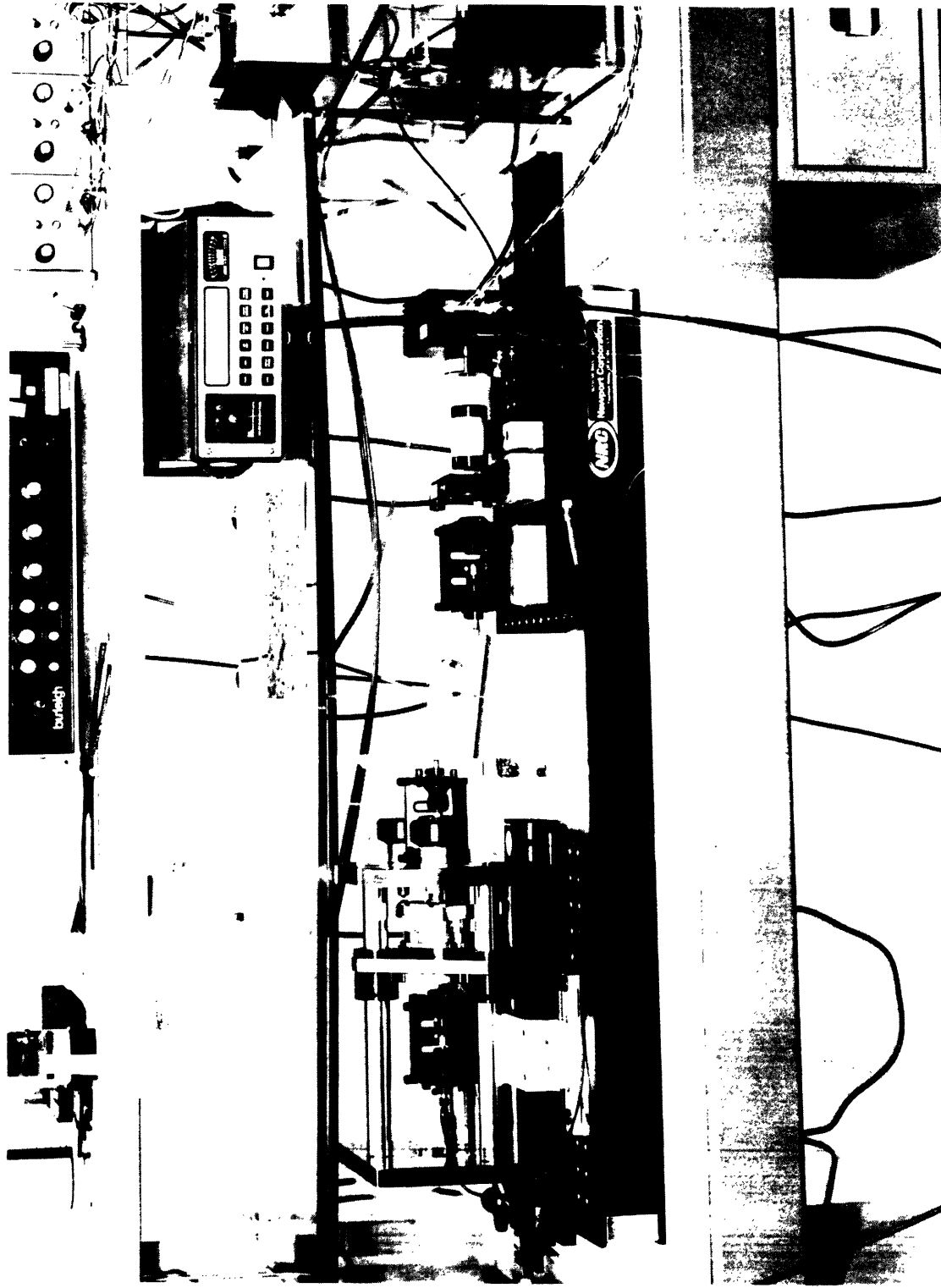systems.

34

Figure 4.1. Launch system.

35

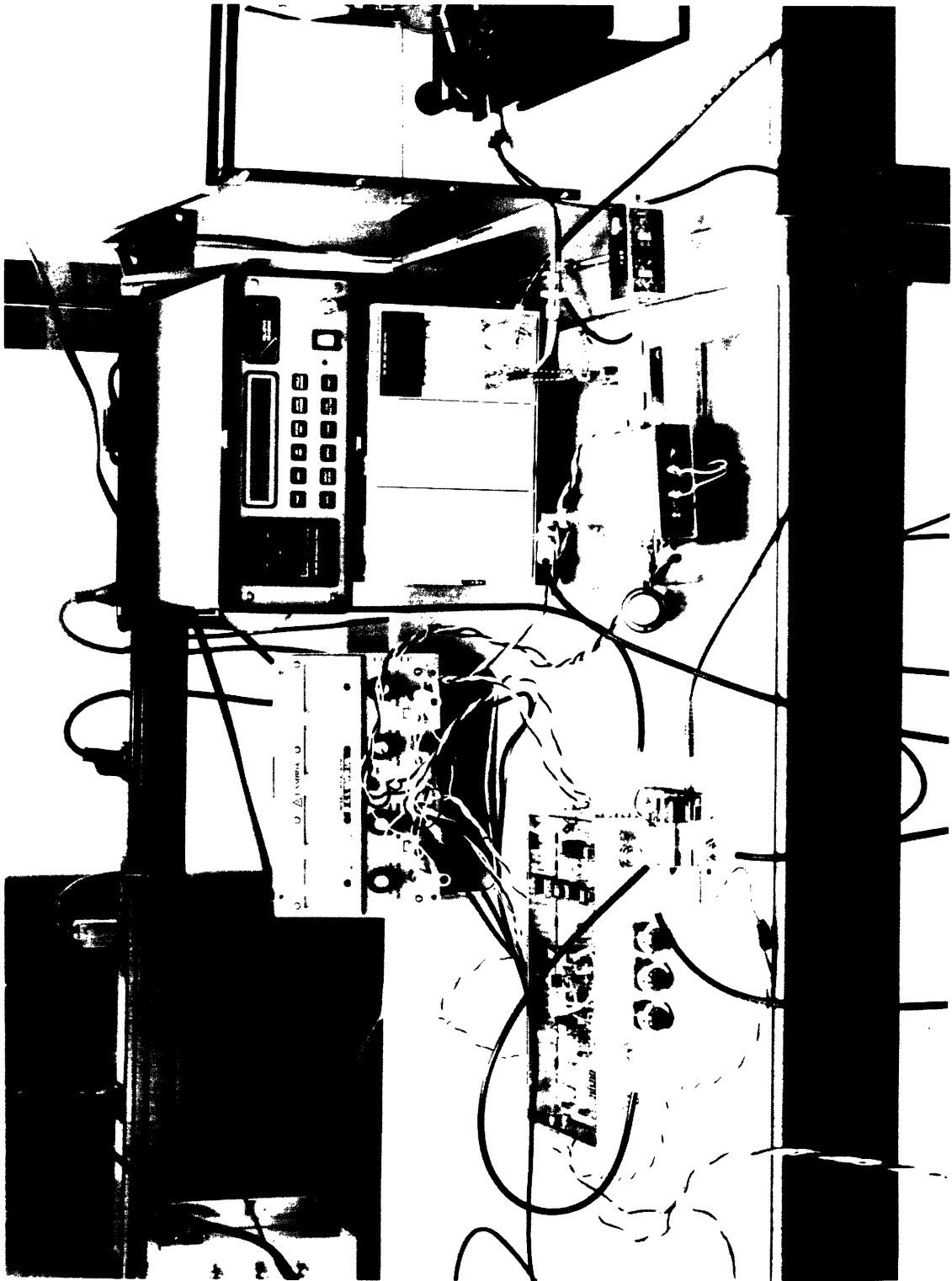Figure 4.2. Launch system and Fabry-Perot.
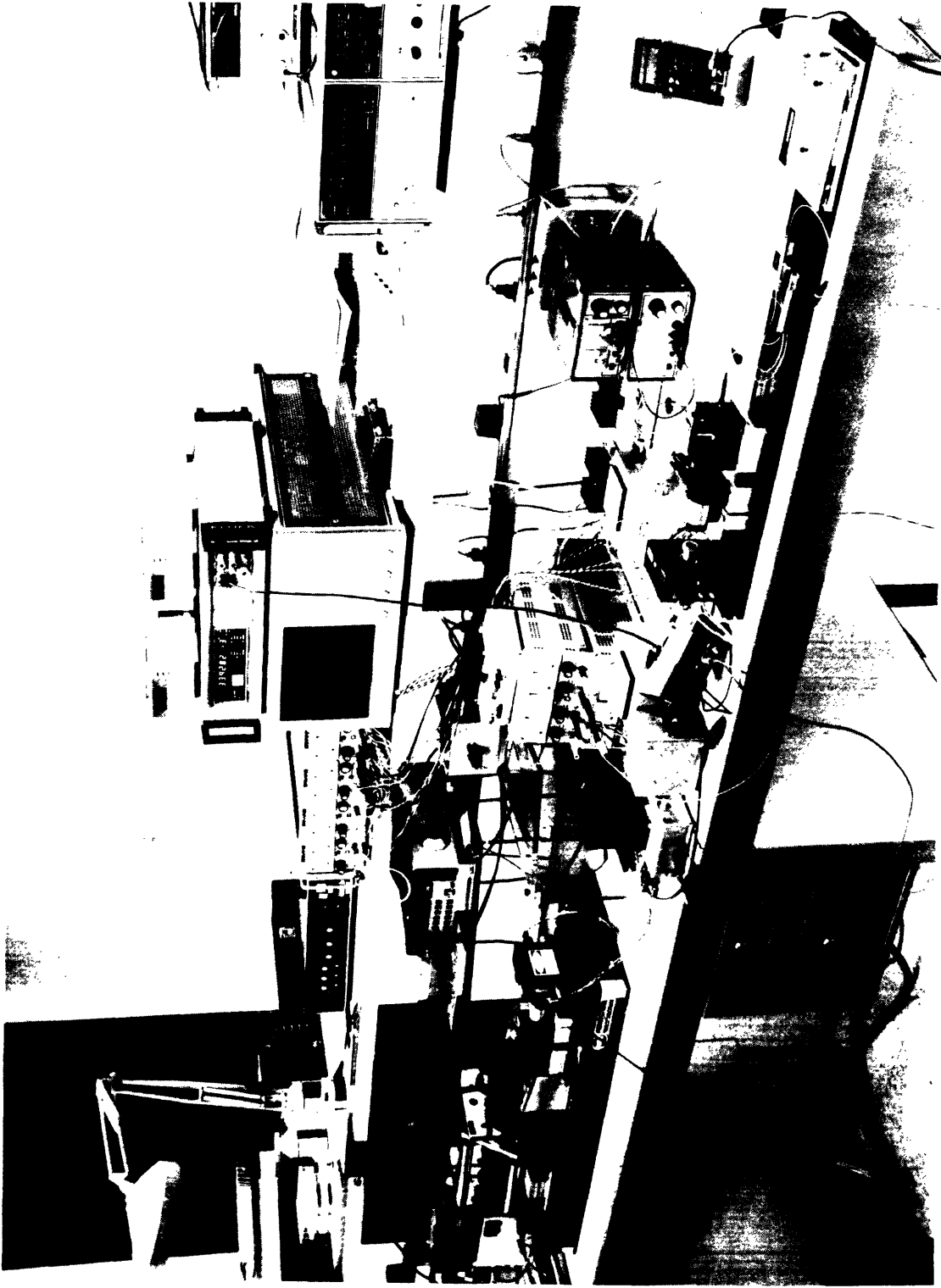
Figure 4.3. Receivers.

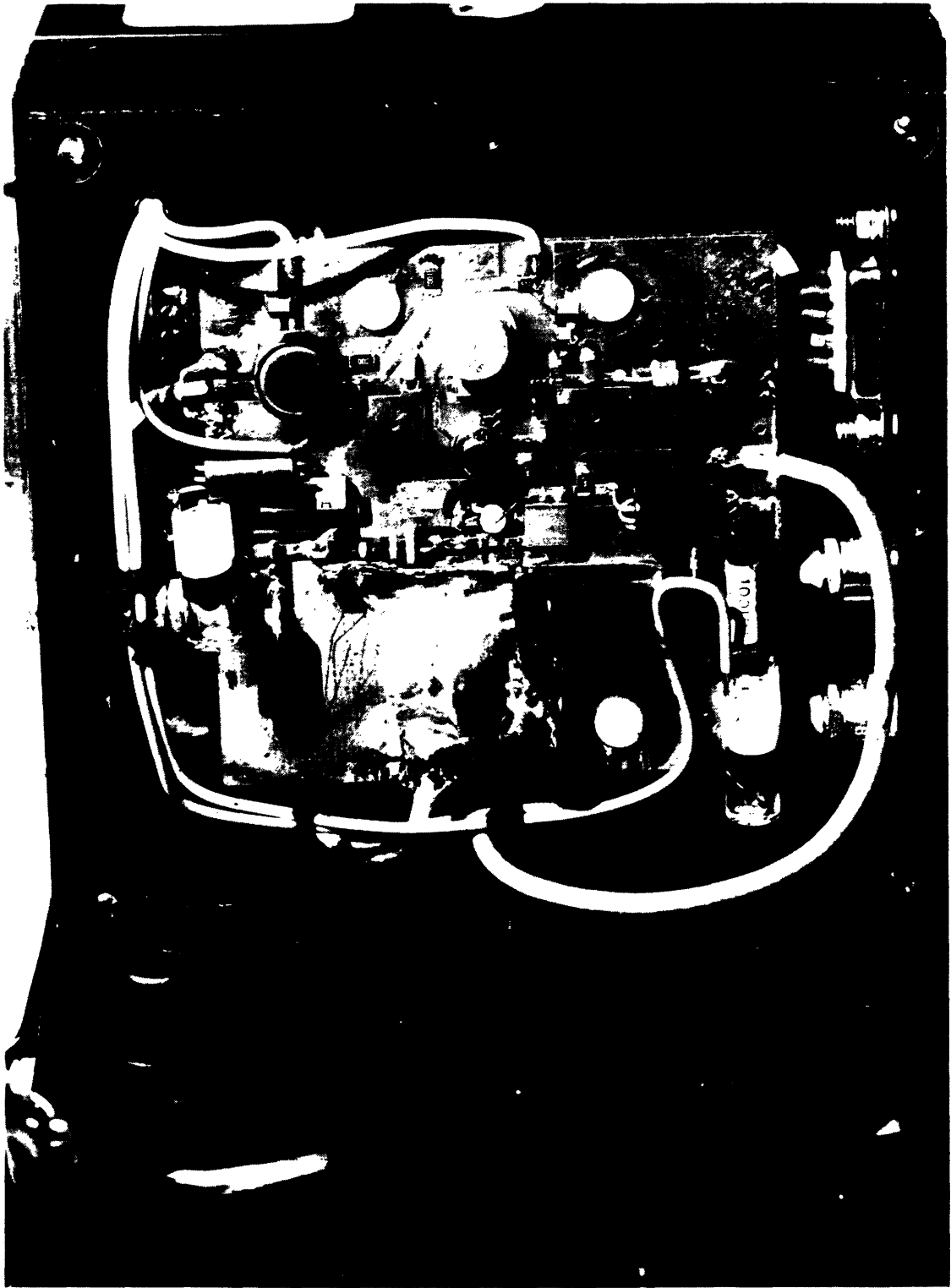Figure 4.4.   Experimental setup.

Figure 4.5. Laser drive circuit.

The two lasers used in this experiment had factory measured wavelengths of 1288 nm and 1289 nm, corresponding to frequencies of 2.3292×10^{14} Hz and 2.3274×10^{14}. This frequency difference of 180 GHz is much larger than any realizable control loop bandwidth, and thus, some forced frequency sweeping would be necessary for acquisition. The rest of this chapter describes how the lasers were tested and an attempt at phase lock was made.

4.3   Linewidth Measurement

The linewidth of the lasers was measured with a fiber inter-ferometer. This interferometer, shown in Figure 4.6, split the light from one laser with an optical coupler. The light then travelled through two different lengths, which decorrelated the noise, and was recombined by another coupler and detected with a wideband receiver. In order to get sufficient decorrelation, the differential fiber length had to be more than five coherence lengths (ℓc) of the laser, since the correlation falls off as $e^{-\Delta L/\ell c}$. The coherence length is directly related to the linewidth by

$$\ell c = \frac{c}{n\Delta f}$$

For the 70-m differential length used, the linewidth can be accurately measured if it is greater than 15 MHz.

The electrical signal from the receiver was observed on a spectrum analyzer. Since the receiver effectively multiplies the two optical signals, the spectrum is the convolution of the spectra of the two signals. The lineshape of the laser spectrum is Lorentzian, with the FWHM defined as the linewidth. Convolving two identical Lorentzians will yield a Lorentzian with a FWHM of twice the individual FWHM. The linewidth of the laser, therefore, is the frequency of the -3 dB point in the convolved spectrum. The photograph in Figure 4.7 show the linewidth of one laser to be 20 MHz.

LASER

DELAY LENGTH

HIGH FREQUENCY RECEIVER
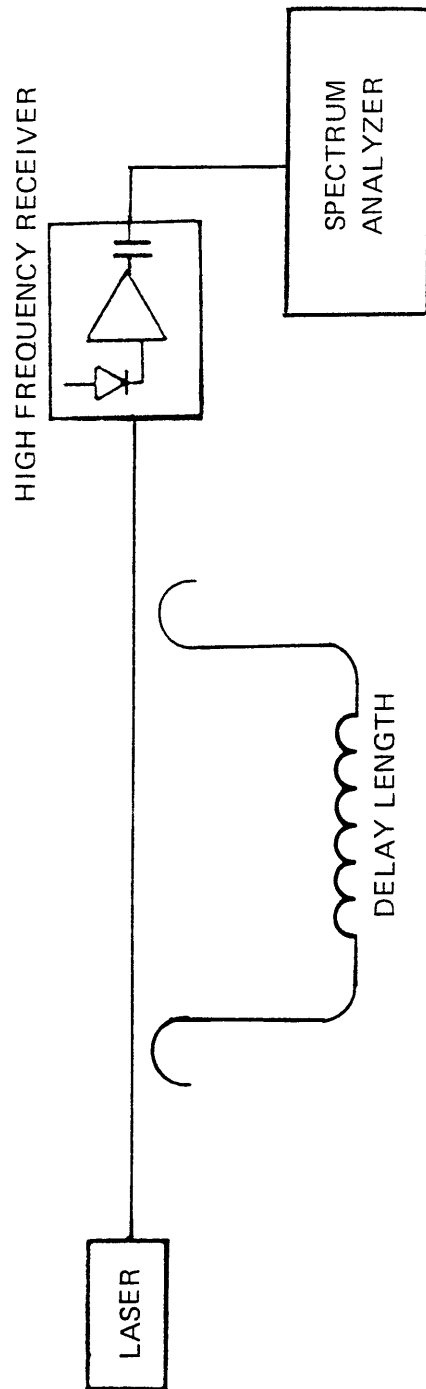
SPECTRUM
ANALYZER

Figure 4.6. Linewidth measurement.
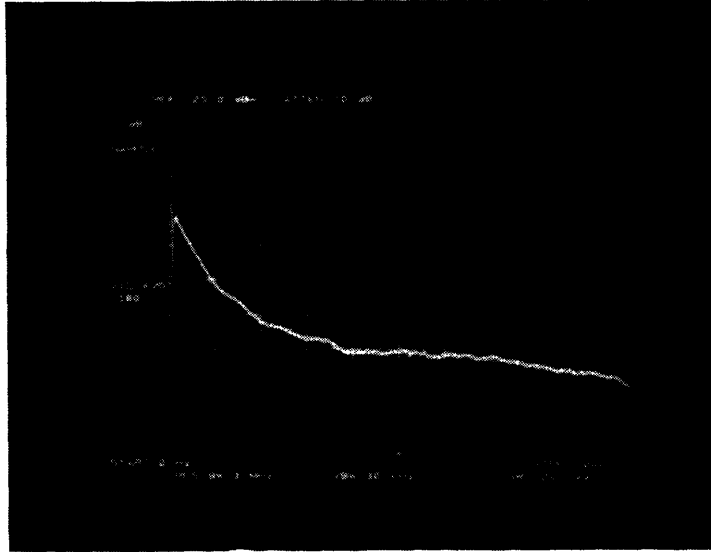
Figure 4.7. Laser linewidth.

The linewidth was found to be very sensitive to injection current and temperature. The 20-MHz linewidth was measured after testing a range of currents and temperatures. In general, a higher current will yield a narrower linewidth for a given temperature. Tuning by current and temperature, though, are subject to mode hopping. This phenomenon, shown in Figure 4.8, is due to the relationship between the cavity resonance modes of the laser, and the gain curve of the medium. As the two are changed by changing the temperature and current, the cavity mode with the highest gain will change in frequency, thus changing the lasing frequency. At some points, though, the lasing frequency will jump from one cavity mode to the next as the gain curve and cavity modes shift by each other. This mode hopping results in discontinuous frequency tuning, shown in the figure. When the lasing frequency is near a dis-continuity, the laser begins to mode hop, and the linewidth becomes wide

42

CURRENT OR TEMPERATURE

FREQUENCY

Figure 4.8. Mode hopping.

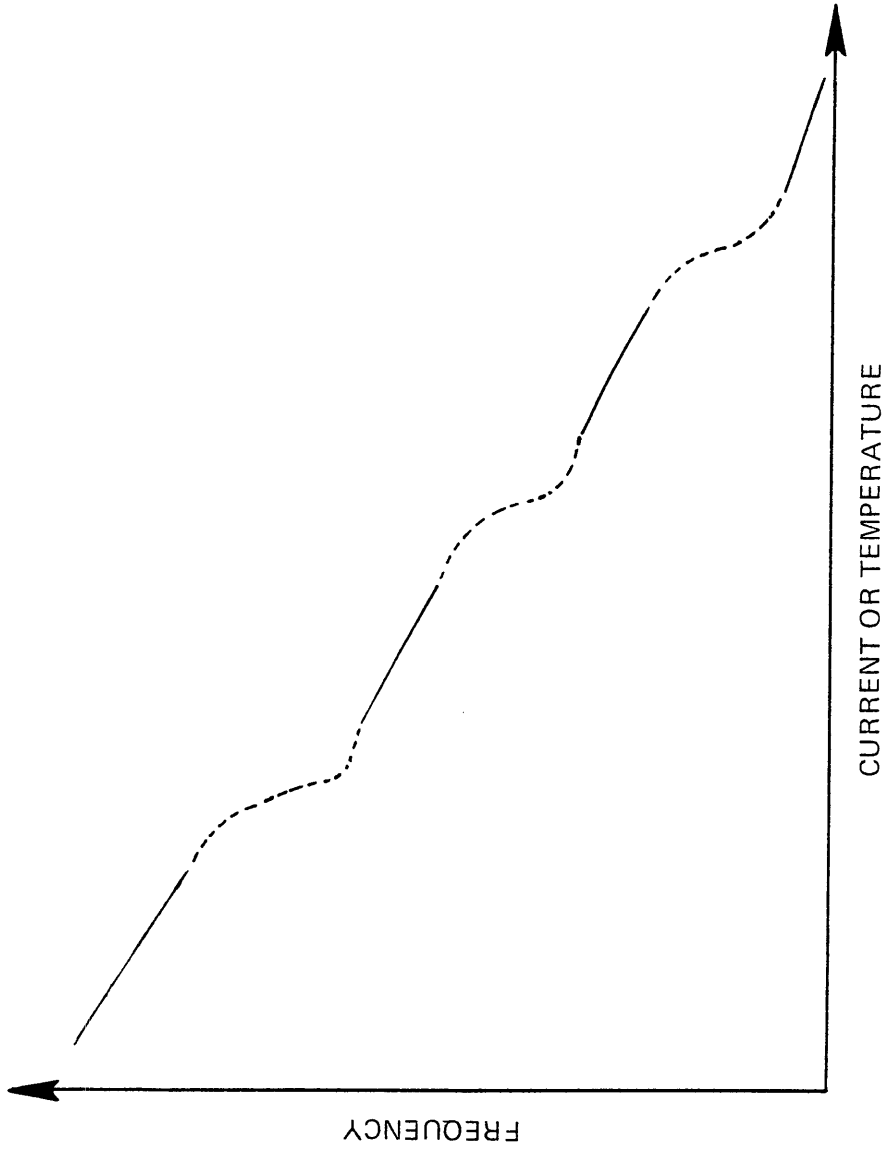and unstable. The various continuous parts of the curve are desired operating points, and offer different stable linewidths. The linewidth varied from 20 MHz to 40 MHz for various points.

A Fabry-Perot interferometer was used to gather data on the lasers. The interferometer had a mirror spacing of 1.24 cm, and thus a free spectral range (FSR) of c/2L, or 12.1 GHz. The expected finesse was about 30, for parallel mirrors. Figure 4.9 shows the experimental setup and result of sweeping the Fabry-Perot mirrors past the laser center frequency. The oscilloscope plot shows the finesse to be

$$F = FSR/(FWHM) = 19.5$$

where FWHM is the full width of the resonance peak at half the maximum value.

The next step in calibrating the laser was to hold the Fabry-Perot mirror spacing still while sweeping the laser center frequency past it. The experimental setup and results are shown in Figure 4.10. The low-frequency current control was driven with a 20-V peak-to-peak, 50-Hz triangular wave, which in turn changed the laser injection current by 1 mA/ms. For such a low frequency, the laser is well-behaved (see below). The Fabry-Perot was then adjusted manually until a peak appeared, to form the oscilloscope plot in the figure. Also in the plot is the triangular drive signal. The width of the resonance at half maximum was known to be FSR/F, or 620 MHz. The scope plot shows that the time to sweep the FWHM was 960 μs, which corresponds to a current change of 0.96 mA. Therefore, the tuning of the laser is 640 MHz/mA for low-frequency modulation.

The temperature tuning of the lasers was also observed by using the Fabry-Perot. Utilizing the computer controlled temperature controller, the temperature was swept over its full range of 10°C to 30°C. The Fabry-Perot peaks were observed periodically, indicating a temperature tuning of the lasing frequency of 25 GHz/°C.
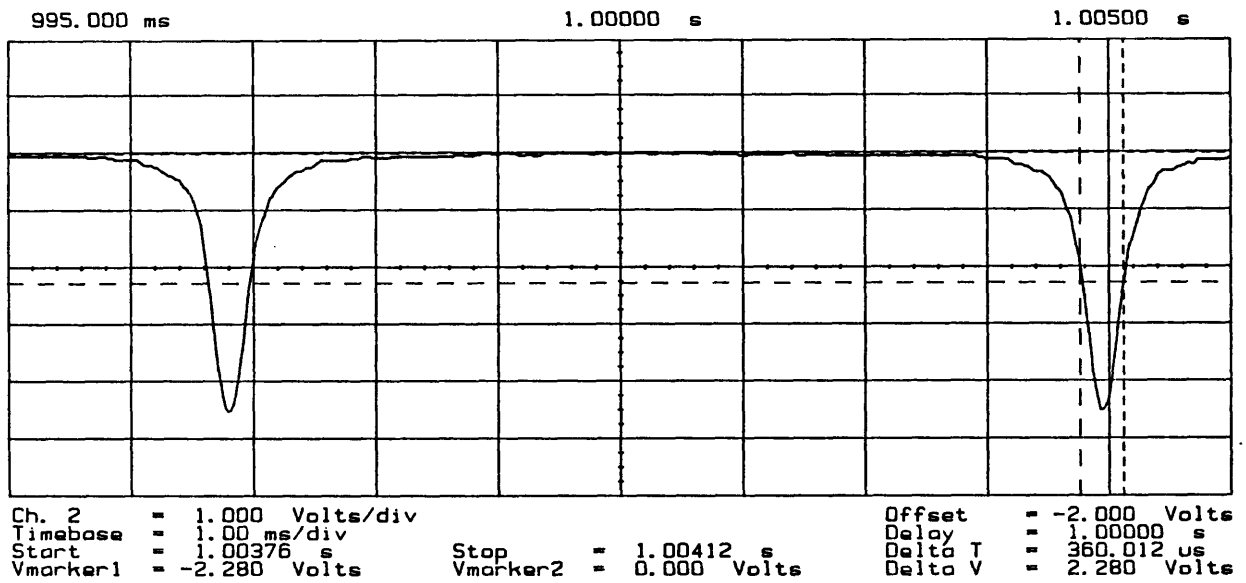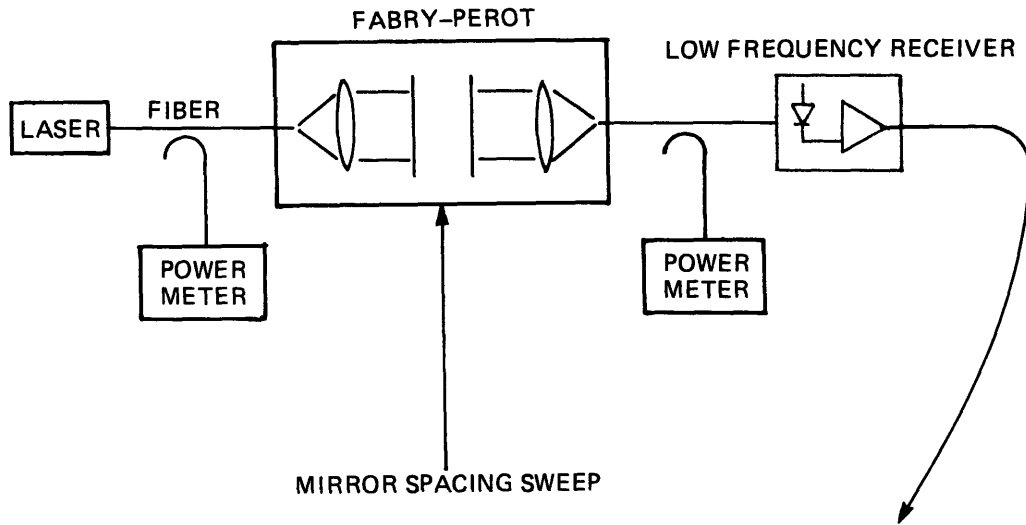
Figure 4.9. Fabry-Perot test setup and results.

FABRY-PEROT

LOW FREQUENCY RECEIVER

LASER FIBER

POWER
METER

POWER
METER

CURRENT SWEEP

0. 00000 s   10. 0000 ms   20. 0000 ms

Ch. 1	=	5. 000	Volts/div			Offset	=	10. 00	Volts
Ch. 2	=	1. 000	Volts/div			Offset	=	-4. 000	Volts
Timebase	=	2. 00 ms/div				Delay	=	0. 00000	s
Start	=	8. 92000 ms		Stop	= 9. 88000 ms	Delta T	=	960. 000	us
Vmarker1	=	-100. 0 mVolts		Vmarker2	= -2. 260 Volts	Delta V	=	-2. 160	Volts

Figure 4.10. Current sweep test setup and results.

46

One final calibration step was used to determine the slope of the Fabry-Perot at the half-maximum point. Around this point the Fabry-Perot acts as a frequency modulation (FM) to intensity modulation (IM) converter. A receiver could then detect the IM optical signal, and would output an electrica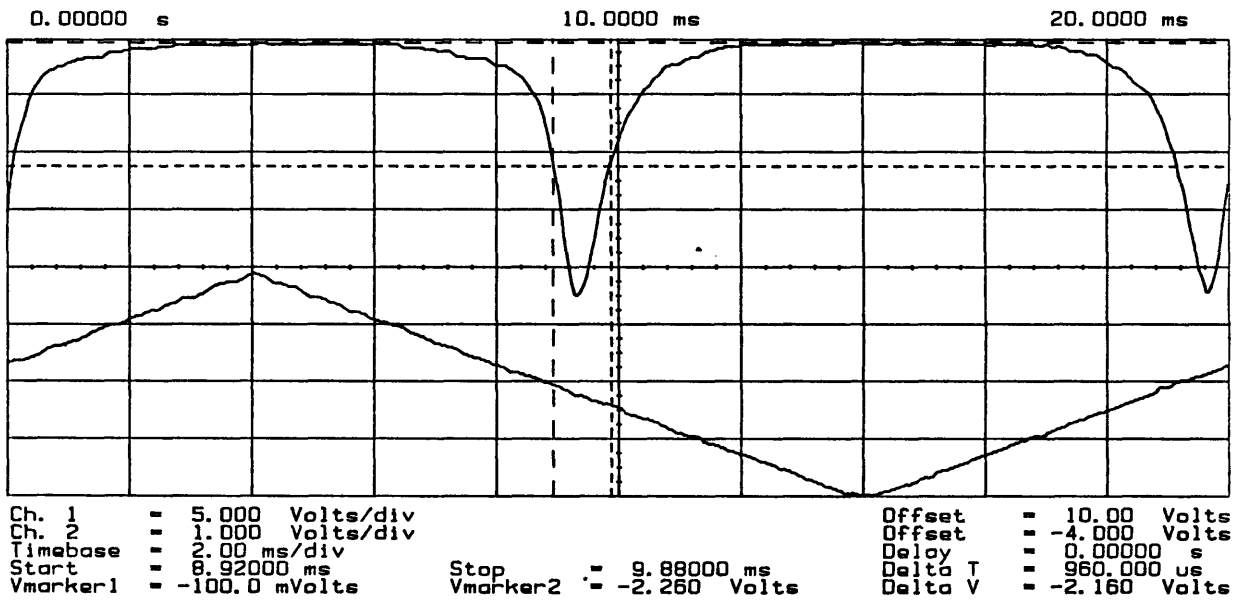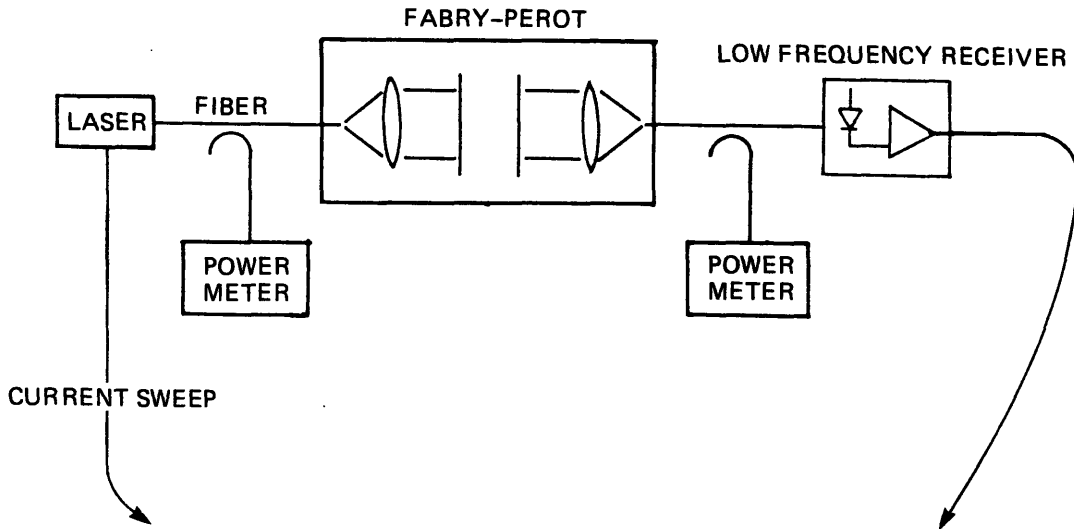l signal at the FM frequency, whose amplitude is proportional to the frequency deviation. The setup in Figure 4.11 was used, only the current modulation was much smaller than for the previous test. After manually adjusting the Fabry-Perot to put the center frequency at the half-maximum point, the low-level modulation was used to determine the slope. For a 0.5-mA amplitude sinewave, the receiver output a 1 V amplitude sinewave. The receiver was known to have a response of 5×10^5 V/W, and thus the Fabry-Perot slope was 6.25×10^{-15} W/Hz.
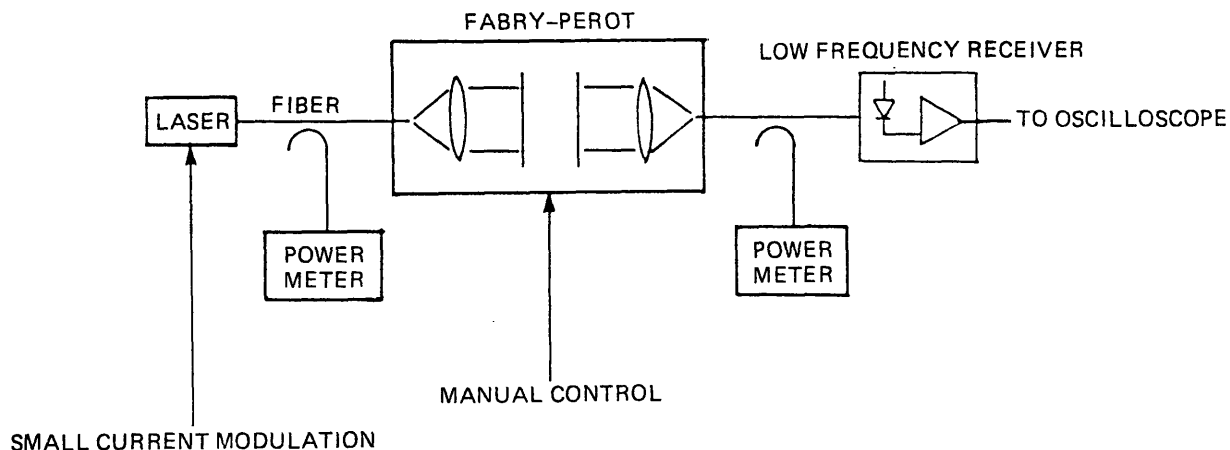
Figure 4.11. Fabry-Perot slope determination.

4.4   Laser Transfer Function

As alluded to earlier, higher frequency modulation of the laser is different from the low-frequency modulation. There are two main effects that determine the center frequency of the laser. One is the size of its resonant cavity, which is very sensitive to temperature. When the temperature rises, the cavity expands, and the lasing frequency decreases. The other effect is the carrier density within the laser, which is directly proportional to the injection current. An increase in

injection current will increase the current density, which will in turn increase the lasing frequency. Unfortunately, increasing the injection current will increase the temperature of the lasing cavity. The result is that at low frequency current modulation the temperature effect domi- nates, while at high frequencies the carrier density effect dominates. At some point, the frequency response of the laser crosses over from one effect to the other, and the result is the frequency response as shown in Figure 4.12. This response was measured with the setup in Figure 4.13 A low-frequency network analyzer was used to drive the low- frequency current control with a variable frequency, low-level signal, which allowed operation on the Fabry-Perot slope. The Fabry-Perot was continually adjusted by an observer to keep the output signal near the half-maximum point. The network analyzer then compared the output to the input to produce the plots in Figure 4.12. Clearly, the laser phase response crosses over around 300 Hz. Also, it is seen that the amplitude response stays constant for the 0 to 100 kHz range. This odd behavior of the laser is modelled by the transfer function for phase

$$G(s) = \frac{K_1(\omega_o - s)}{s(\omega_o + s)}$$

where

$\omega_o = 2\pi * 300$ Hz, the phase crossover frequency

$K_1 = 640$ MHz/mA

4.5 Frequency Lock to the Fabry-Perot

The first feedback loop attempted was to frequency lock a laser to the half-power point on the Fabry-Perot resonance curve. The setup is shown in Figure 4.14 with the control block diagram. The Fabry-Perot
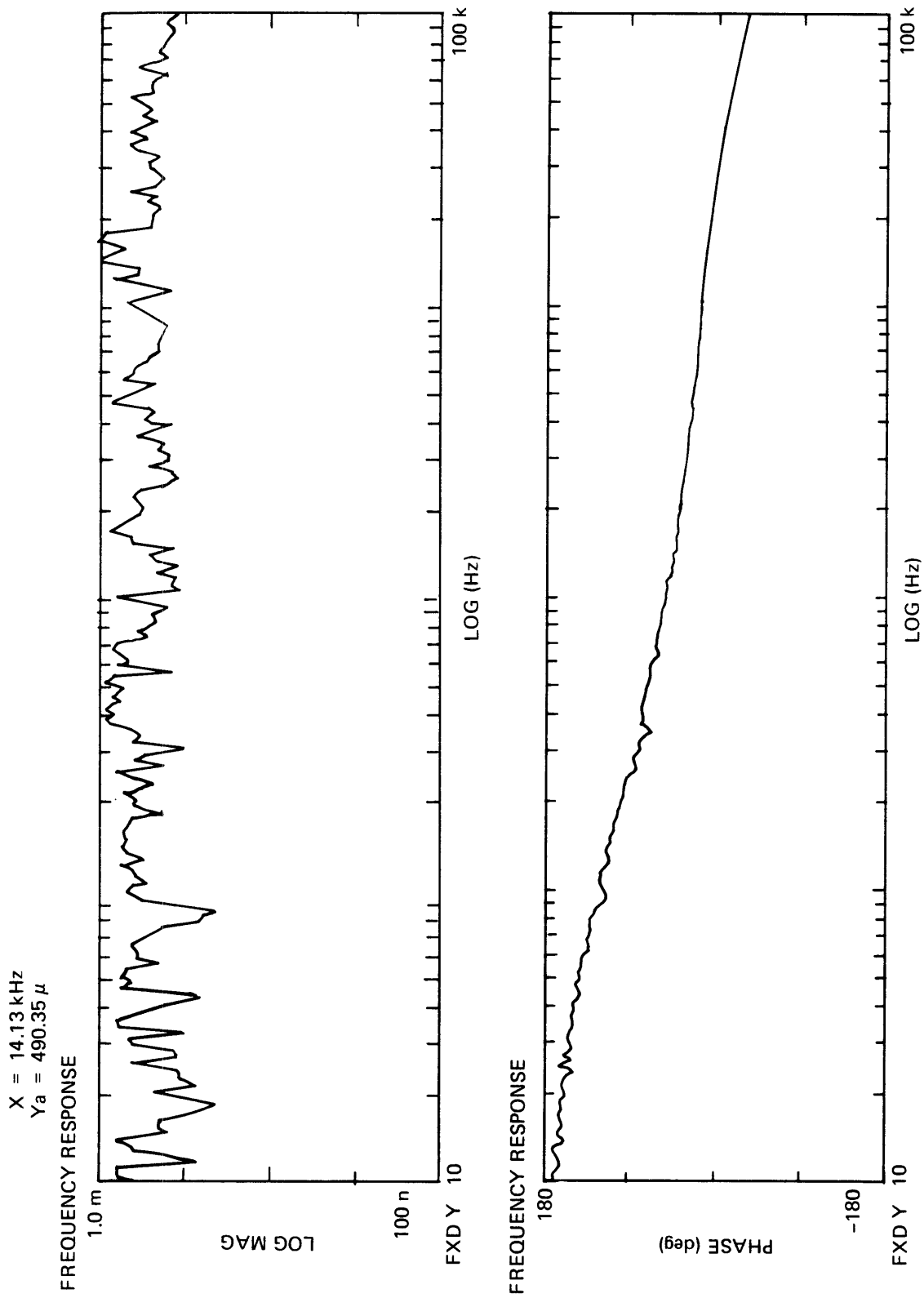
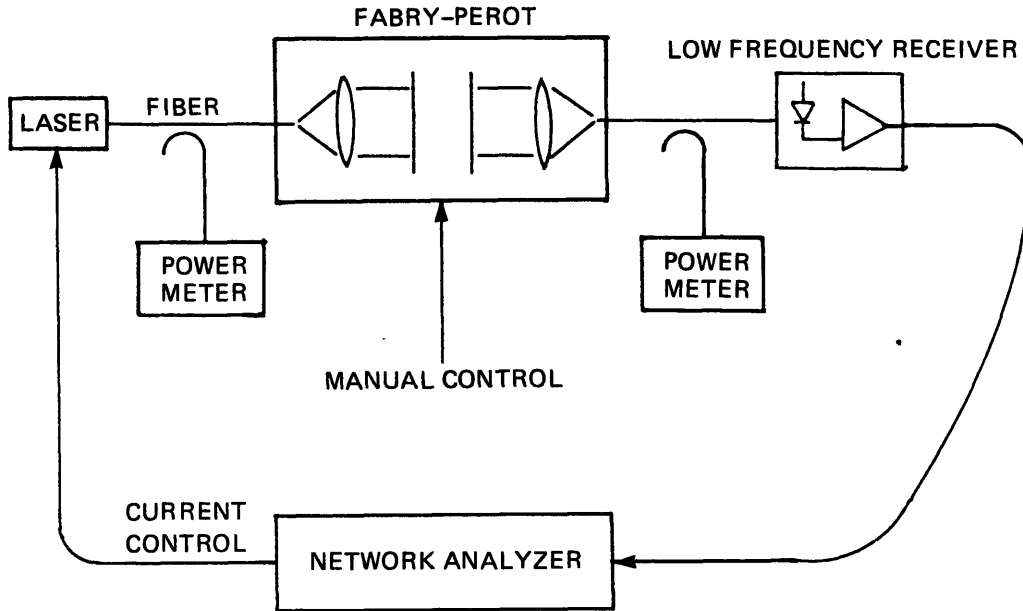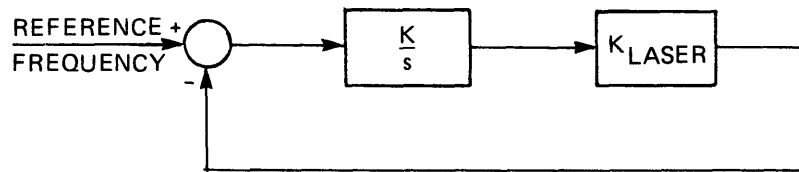Figure 4.12. Frequency response of laser diode.

49

Figure 4.13. Frequency response test setup.

and receiver acted as a frequency comparator, yielding a signal propor-
tional to the frequency deviation from a set point. An op-amp
integrator was the loop filter, and the laser frequency was controlled
by the low frequency current control.

The loop compensation was adjusted by varying the gain of the op-
amp integrator circuit. By adding an input into the loop at the op-amp,
the closed loop response was observed at the output of the receiver.
First, a slow square wave was used, in order to observe the step re-
sponse. The loop gain was then adjusted until the response shown in
Figure 4.15 was achieved. The small bump in the response that goes in
the wrong direction is due to the 180° phase shift of the laser fre-
quency response for high frequencies. Next, by using the low frequency
network analyzer, the closed loop transfer function was measured, as
shown in Figure 4.16. The loop bandwidth was about 100 Hz. This was
expected since the extra phase shift from the laser was 90° at 300 Hz,

50

FABRY–PEROT

LASER | FIBER

POWER METER

SET POINT

LOW FREQUENCY RECEIVER

CURRENT CONTROL | COMPENSATION

REFERENCE FREQUENCY $+$ $-$

$\dfrac{K}{s}$
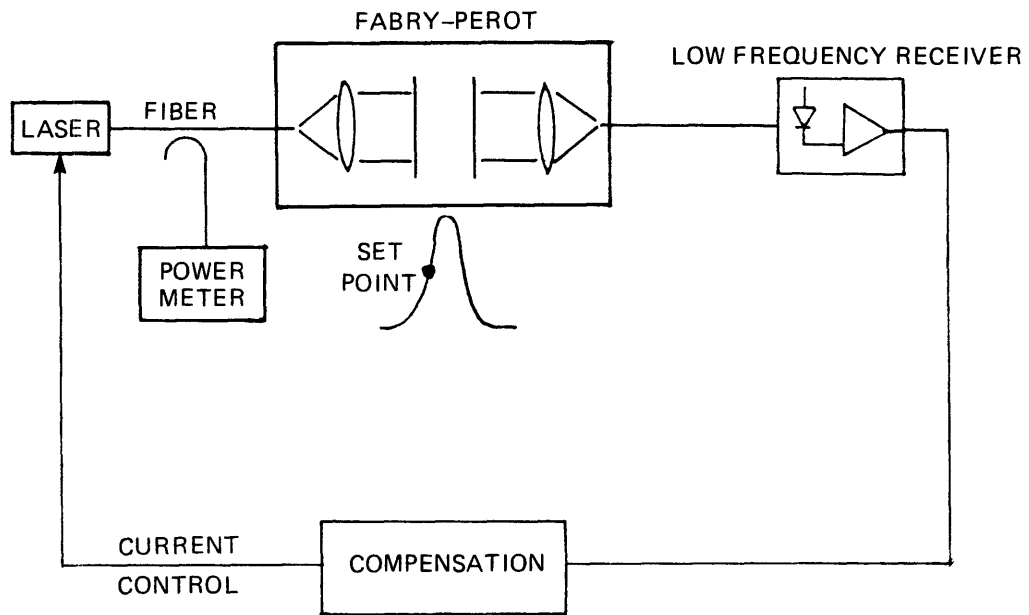
K_{LASER}

$$G(s) = \frac{K}{s} K_{LASER}$$

Figure 4.14. Frequency-locked loop.

```
Ch. 1       =   500.0 mVolts/div                          Offset  = -1.160   Volts
Ch. 2       =   500.0 mVolts/div                          Offset  =  1.220   Volts
Timebase    =    10.0 ms/div                              Delay   = -259.040 ms
Channel 1 Parameters           Rise Time  =  811.756 us
Start       =  -248.640 ms     Stop       = -247.828 ms   Delta T = 811.756 us
Vmarker1    =  -320.0 mVolts    Vmarker2  =  280.0 mVolts  Delta V = 600.0 mVolts
```
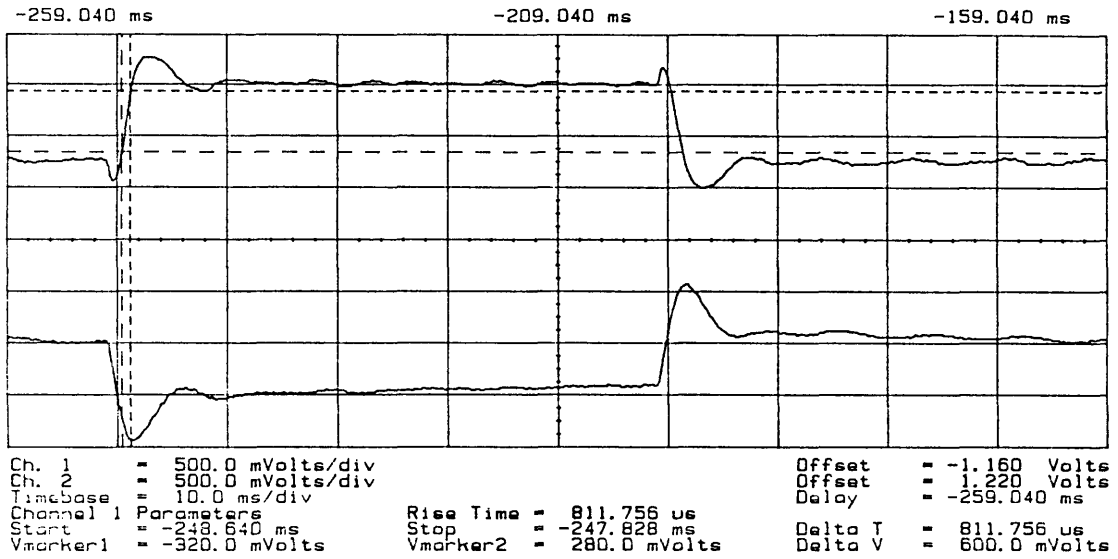
Figure 4.15. Step response of frequency lock.

X=568.9 Hz

FREQ RESP

Log Mag

Fxd Y 10   Log Hz   100k

Yb=-37.37 Deg

FREQ RESP

Phase

Deg

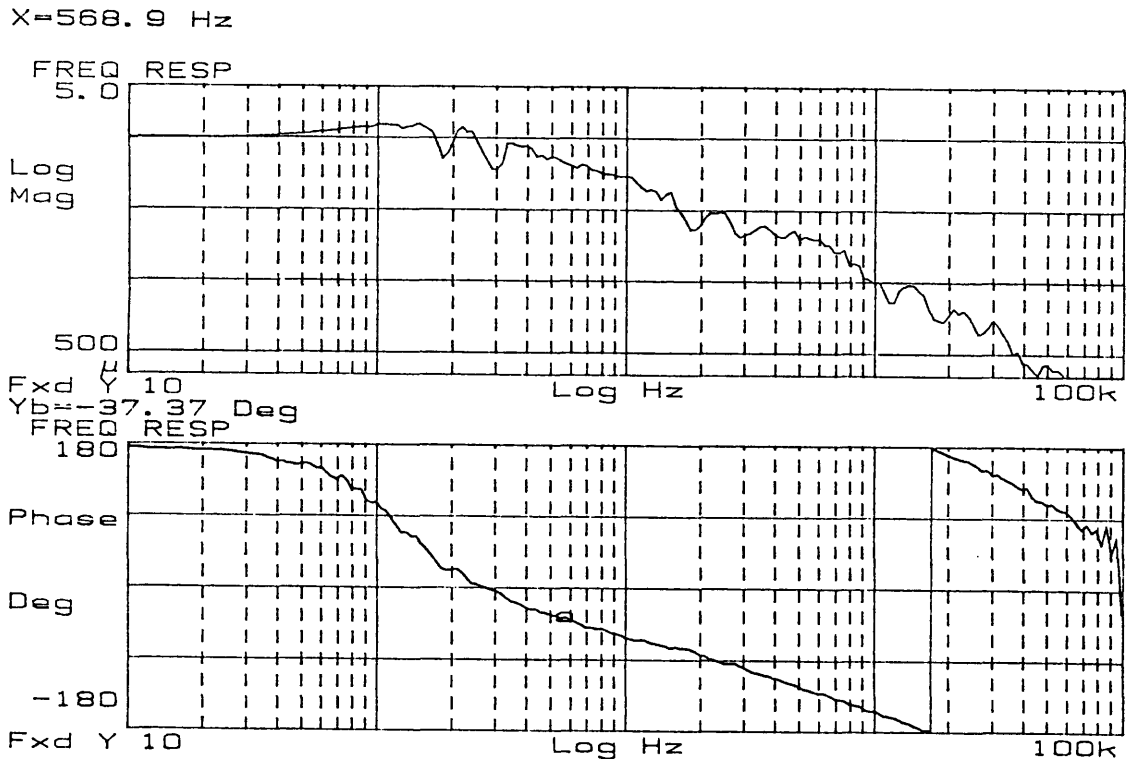Fxd Y 10   Log Hz   100k

Figure 4.16. Closed loop transfer function of frequency lock.

52

and this would be about 20° at 100 Hz. For a crossover frequency of G(s) of 100 Hz, the phase of G(s) would therefore be -90° − 20°, or -110°. This leaves a phase margin of 70°, which corresponds to the observed step response.

After locking the laser to the Fabry-Perot, it became obvious that the power supplies used for the electronics were contributing a 120-Hz buzz to all of the signals. The evidence was a strong 120-Hz signal on the output of the receiver when the loop was locked. To deal with this problem, all possible circuits were run off ±12-V batteries instead of the usual power supplies. This considerably reduced the 120-Hz buzz. There was still some, however, since the Fabry-Perot mirrors and the temperature control circuits were still supplied from the 60-Hz laboratory supply.

4.6   Laser Frequency Noise

The frequency noise of the laser diodes has a theoretical spectral density as shown in Figure 4.17. The 1/f corner frequency was measured by the setup in Figure 4.18. The laser was locked to the Fabry-Perot slope by a narrow (0 to 100 Hz) feedback loop, and the output of the receiver was examined on a spectrum analyzer. The photo in Figure 4.19 shows the 1/f corner to be at 67 kHz, and the white noise continuing afterwards. The white noise drops off starting around 200 MHz because the Fabry-Perot acts like a low-pass filter with a cutoff of 250 MHz. It is assumed, though, that the white noise continues as theory predicts. The transfer constant for the wideband (10 kHz to 1 GHz) receiver used in the high-frequency picture was 1 mV/μW electrical power to light power. Thus, the white frequency noise had a strength of 1.02 MHz^2/Hz. In terms of the laser linewidth, this converts to a 32 MHz linewidth.

4.7   Laser Frequency Overlap

The next step toward phase lock was to tune the laser frequencies with temperature in order to get them to overlap. Figure 4.20 shows the experimental setup. The light from the two lasers was combined with a coupler, then detected using the high frequency receiver. The result
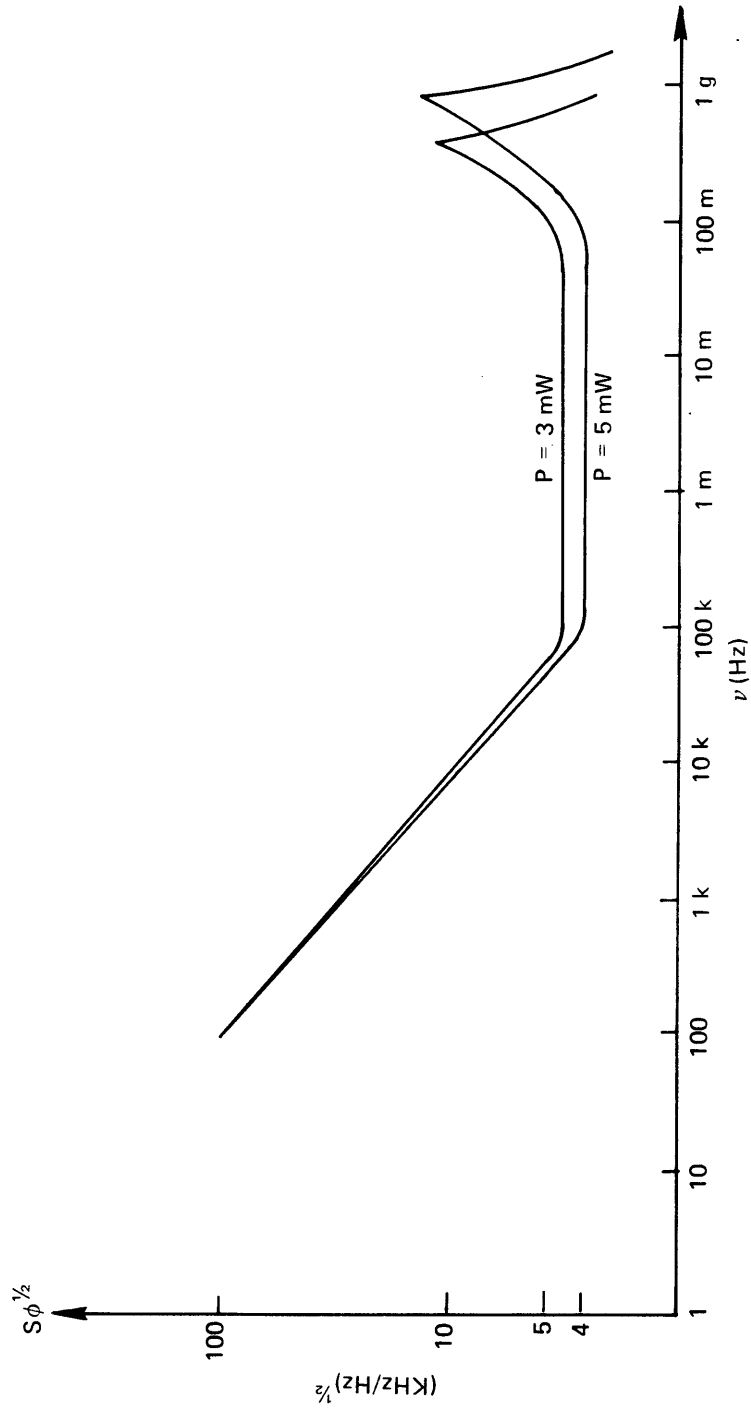
53

Figure 4.17. Theoretical laser frequency noise spectrum.
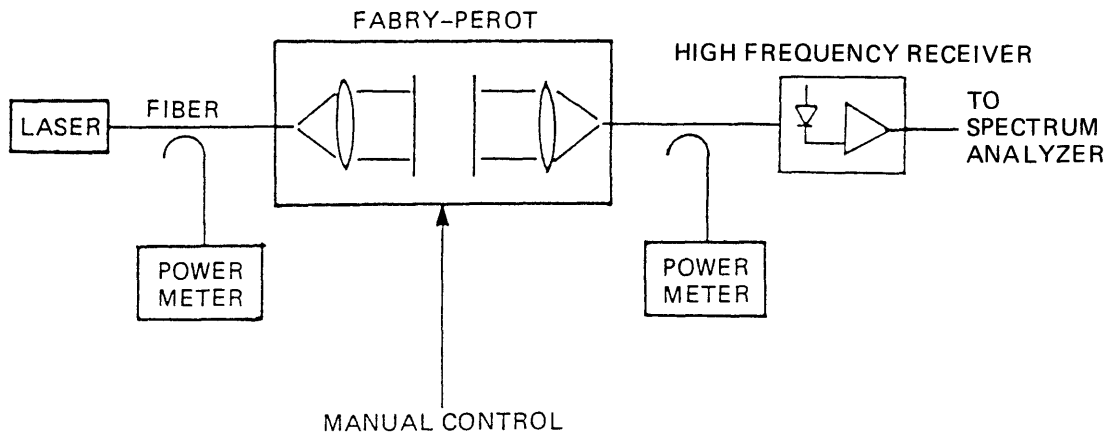
Figure 4.18. Frequency noise measurement.

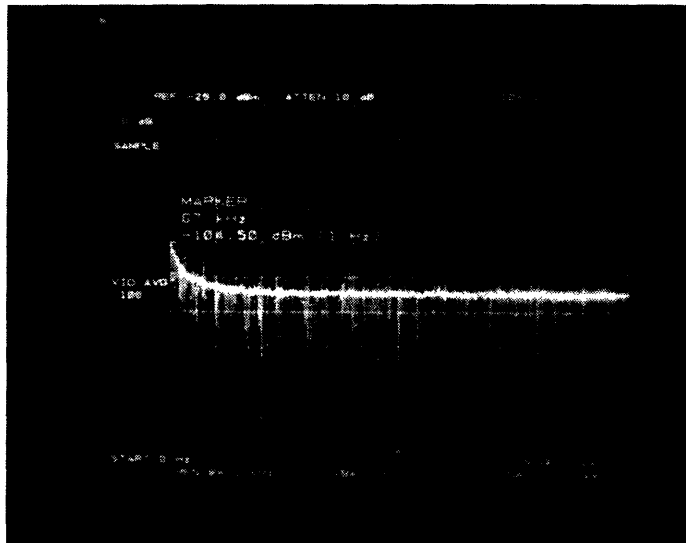Figure 4.19. Frequency noise.

was the convolution of the spectra of the two lasers, as in the line-
width measurement, but offset from zero by the difference in frequencies
between the two lasers. Since the lasers were about 180 GHz apart at
25°C (from the data sheets), and then tuned approximately 25 GHz/°C, a
temperature difference of around 7°C should have tuned the frequencies
to the same value.

HIGH FREQUENCY RECEIVER

LASER

LASER

TEMPERATURE CONTROL
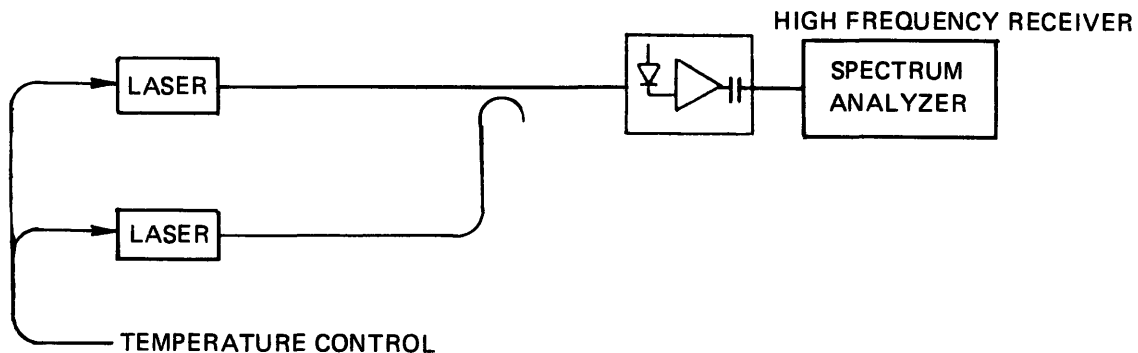
SPECTRUM
ANALYZER

Figure 4.20. Laser frequency overlap setup.

Using the computer control of temperature, a 14°C difference was
found to produce a difference frequency, or beat note, of less than 1
GHz. Figure 4.21 shows the spectrum when the difference is 700 MHz.
The mutual linewidth was measured to be 140 MHz, which meant that the
individual linewidths were 70 MHz if they were equal. This picture was
taken before the 120-Hz buzz was removed from the circuitry, so the beat
note actually was jittering around at 120 Hz. Also, no attempt was made
at this time to optimize the linewidths of the lasers through fine
current adjustments as was done before.

Figure 4.21. Laser frequency overlap.

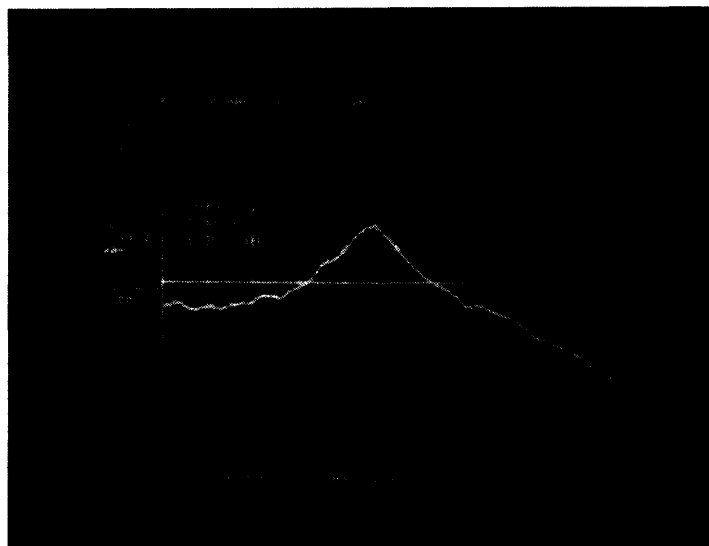Another frequency locked loop was attempted in order to remove the 120-Hz jitter in the difference frequency. The output of the high frequency receiver was sent through an electrical delay line discriminator. The discriminator worked like the Fabry-Perot in that it converted frequency deviations to intensity deviations, only it operated on an electrical signal instead of an optical signal. This signal was then filtered as before with an op-amp integrator. The filtered signal then drove the low frequency current control of the laser. Unfortunately, the 180° phase shift of the laser prevented the loop from tracking the 120 Hz, since the loop was limited to less than 100 Hz.

After the 120-Hz problem was solved by using batteries as power supplies, frequency overlap was attempted again. Due to an unfortunate accident involving turning the power to the laser on and off, one of the lasers had an order of magnitude increase in its linewidth, shown in Figure 4.22. The spectrum of the beat note then looked like wideband white noise with a small bulge at the beat note. No amount of linewidth reduction through current adjustment could improve the beat note. One week later, the laser had degraded even more, and the beat note was no longer distinguishable on a 0 to 1.5-GHz scale.
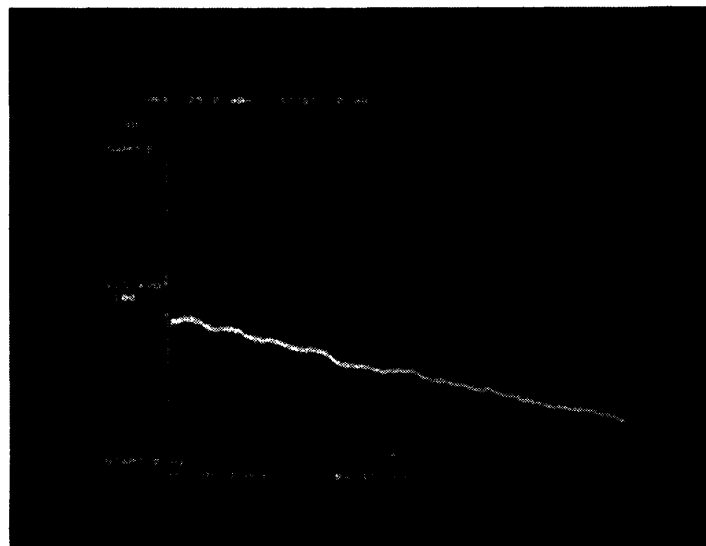

Figure 4.22. Poor laser linewidth.

CHAPTER 5

PHASE LOCK RECOMMENDATIONS

5.1   Loop Bandwidth and Noise

The experiments in Chapter 4 allow Equation (11) from Chapter 2 to be evaluated. This equation, reproduced here, relates the phase error variance to the noises in the loop.

$$\sigma^2 = \frac{\pi}{2K^2}(N_{yb} + N_{3b}) + \frac{1}{2K}(N_{ya} + N_{3a}) + \frac{K}{2}(\frac{N_1}{K_1^2} + \frac{N_2}{K_1^2 K_2^2}) \quad (11)$$

The laser noises were measured in Chapter 4. For simplicity, the noise statistics for the better laser are used. The white frequency noise was measured to be $N_{ya} = N_{3a} = 3.2 \times 10^7$. Since the $1/f$ laser noise equalled the white noise at 67 kHz, $N_{yb} = N_{3b} = 1.3 \times 10^{12}$. The noise from the detector, N_1 was measured to be $N = 8 \times 10^{-11}$. Finally, the electrical noise N_2 was not measured, but would be about $N_2 = 10^{-11}$.

Two of the three gains were measured, and the third, K_2, would be varied in order to control the total loop gain $K = K_1 K_2 K_3$. The laser gain was measured to be $K_3 = (640 \text{ MHz/mA})(0.5 \text{ mA/V}) = 3.2 \times 10^8$ Hz/V. The detector gain was measured to be $K_1 = 1/2 \quad P_1 P_2 \ (5 \times 10^5) = 5 \times 10^6$. Substituting these values into Equation (11) yields

$$\sigma^2 = \frac{4 \times 10^{12}}{K^2} + \frac{3.2 \times 10^7}{K} + K\left[3 \times 10^{-24} + \frac{4 \times 10^{-25}}{K_2^2}\right] \quad (17)$$

where K is the loop gain, and also the open loop crossover frequency. For values of K less than 1 GHz, the variance is dominated by the laser frequency noise, and Equation (17) reduces to

$$\sigma^2 = \frac{N}{K} = \frac{3.2 \times 10^7}{K} \qquad (18)$$

Thus, the loop bandwidth K must be greater than the laser linewidth N for phase lock to take effect. To achieve this wideband loop, both the low and high frequency receivers and the low and high frequency current sources for the laser diode would be used. Unfortunately, the 180° phase shift measured in Chapter 4 cannot be compensated out and still leave the desired loop filter. This phase shift is typical of most semiconductor lasers. It is often observed at much greater frequencies, up to 10 MHz, but a 20-MHz linewidth would require it to be more than 100 MHz for phase lock. There are new lasers, however, that do not exhibit this troublesome phase shift. As reported in References 9 and 10, the new devices rely upon multi-electrode diodes and a more complicated drive circuit. The use of these lasers might allow a semiconductor laser phase locked loop.

An alternative scheme is described in Section 5.3, but first the expected results of a phase lock experiment are discussed in Section 5.2.

5.2   PLL Results

Figure 5.1 shows the expected spectrum of the error signal as the PLL is improved. First, Figure 5.1a shows the Lorentzian mutual linewidth of the two lasers at an arbitrary offset frequency. Figure 5.1b shows the spectrum at a zero offset frequency, when the lasers are frequency locked. As the gain of the loop is measured, more frequency noise is removed by the loop, since the bandwidth is increased. Figure 5.1c shows how the spectrum changes as the loop gain is increased. At some point, the phase error variance becomes small enough so that the
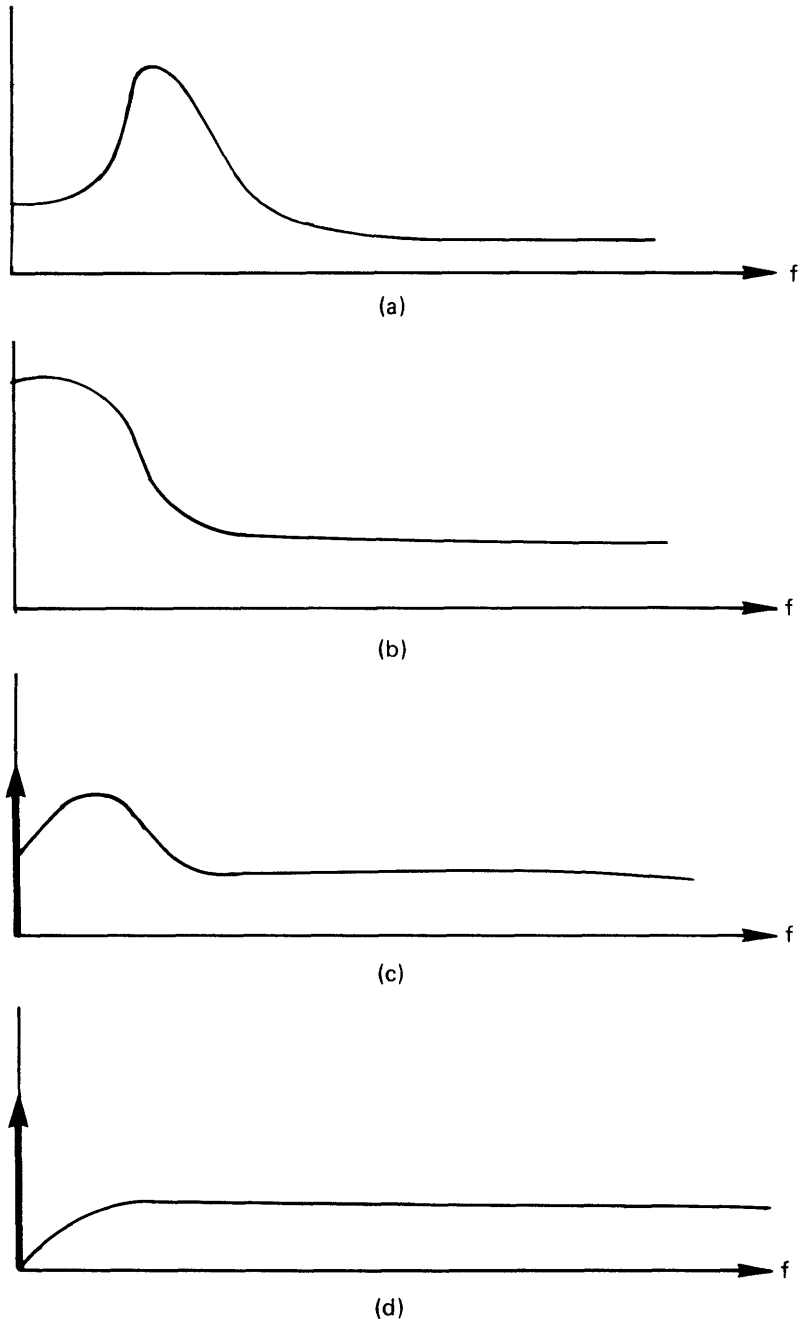
Figure 5.1. Spectra of PLL error signal.

sinusoidal phase detector can be considered linear. This point also corresponds to successful phase lock. The spectrum here is shown in Figure 5.1d. The area under this curve is the phase error variance.

5.3   Phase Modulator in the PLL

Figure 5.2 shows a scheme for realizing a PLL by incorporating an electro-optic phase modulator into the previous setup. The phase modulator can function as a frequency shifter, as described below. By using the phase modulator instead of the laser current as the wideband feedback path, any problems with the laser frequency response can be avoided.

The phase modulator consists of a substance with a controllable index of refraction. Applying a voltage across the substance, a titanium diffused lithium niobate waveguide, achieves this change. Since the speed of the light depends upon the index of refraction, the time to travel the length of the waveguide is controlled, and thus the phase is controlled. By applying a ramping voltage to the phase modulator, a frequency shift is attained, since a linearly increasing phase is equivalent to a frequency shift. One problem is that it is not feasible to ramp the voltage forever. The solution is to take advantage of the fact that an instantaneous 2π phase shift of a sinusoid corresponds to no change in phase. Therefore, a sawtooth waveform, as shown in Figure 5.3, will cause the desired frequency shift. This technique is called serrodyning.

The difficulty in using serrodyning in the PLL is the creation of the serrodyne waveform. High frequency, fast 2π flyback serrodyne waveform generators are currently under development at Draper Laboratory, and would be ideal for use in the PLL.

5.4   Simplified PLL Test

Figure 5.4 shows a way to use only one laser to test the PLL, which includes phase modulators. The laser light is split into two paths which are treated as the two independent oscillators. One path is
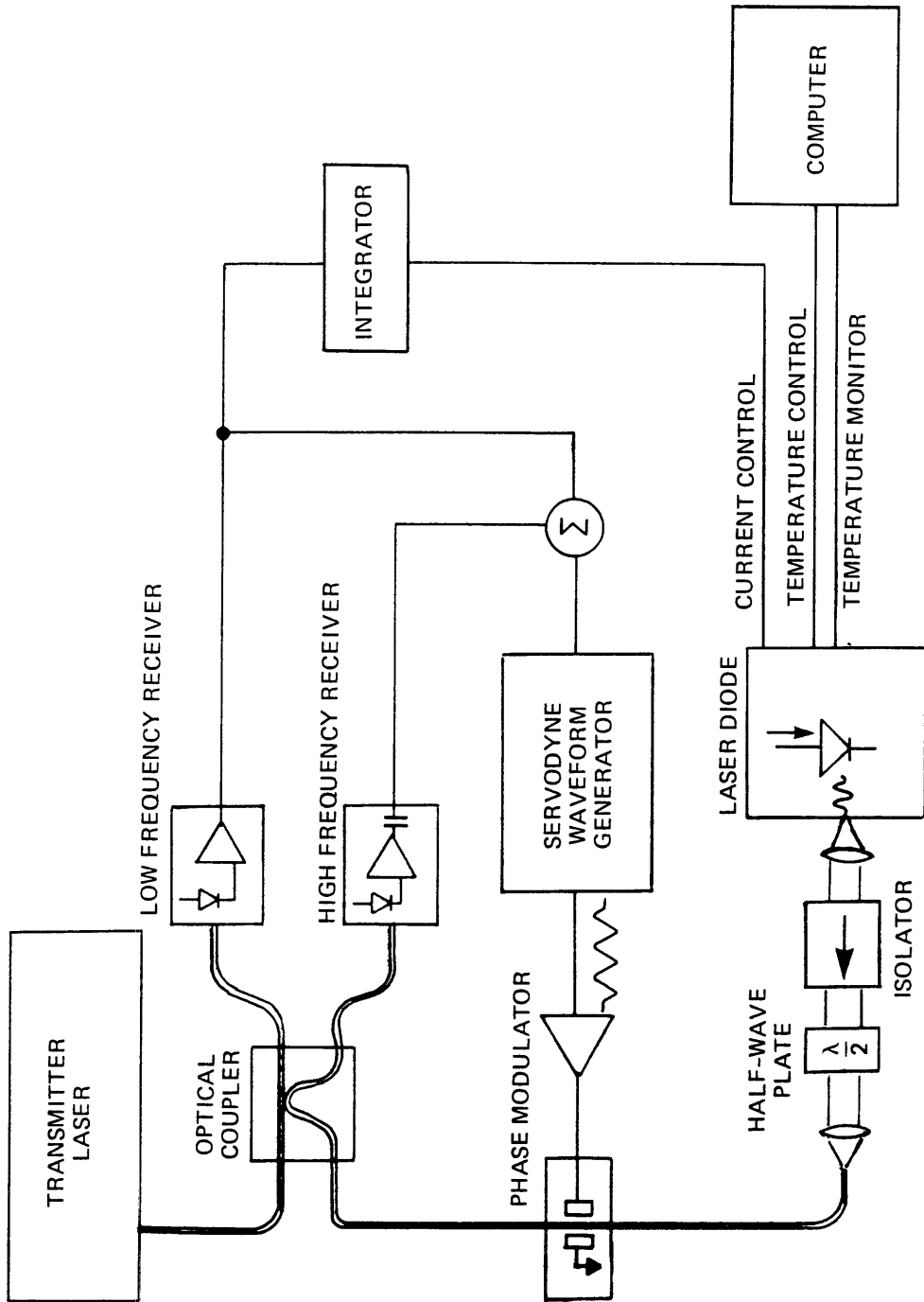
Figure 5.2. PLL using phase modulator.
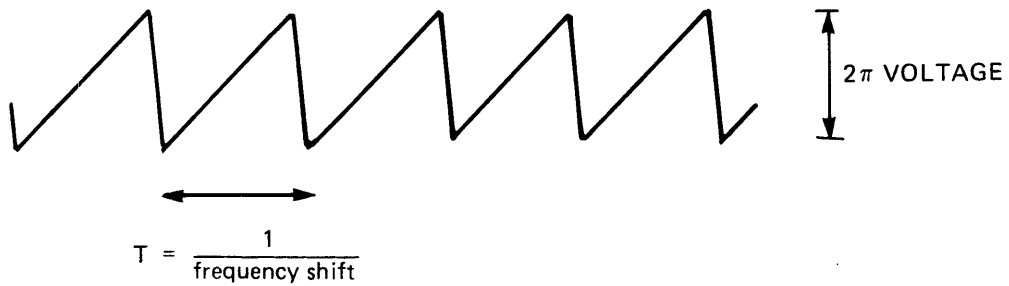
$$T = \frac{1}{\text{frequency shift}}$$

Figure 5.3. Serrodyne waveform.
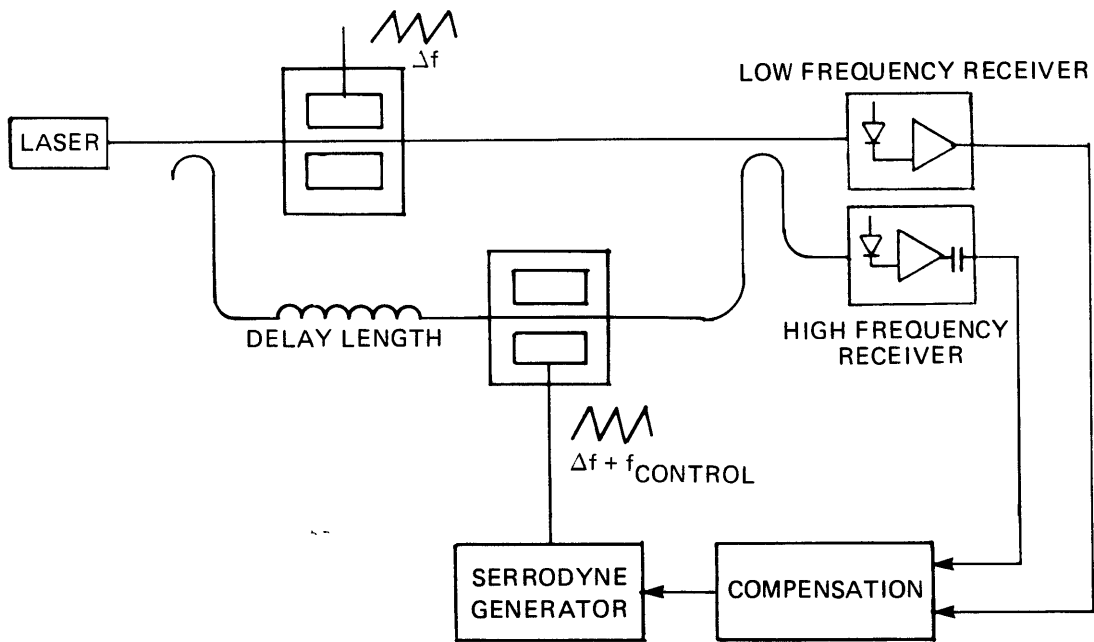
Figure 5.4. Simple phase lock test.

frequency shifted by the serrodyne technique. The other path is first delayed in order to decorrelate the noise from the first path, then frequency shifted by the same amount by a controllable serrodyner. The signals are then combined and detected as before. The feedback is through the same compensation as before, and drives the controllable serrodyner. The two paths are frequency shifted because it is simpler

to create an adjustable sawtooth wave that only ramps up or down, but not both. One advantage to using only a single laser is that frequency lock is no longer a dynamic range issue. Also, the delay length can be adjusted in order to control the amount of noise decorrelation, and thus the apparent noise bandwidth that the loop must track out.

CHAPTER 6

CONCLUSIONS

This thesis has presented the major design issues involved in an optical phase locked loop. The main source of error in the phase lock was identified as the white frequency noise of the lasers, which is proportional to the laser linewidth. Other concerns are the tunability and frequency response of the lasers, the linewidth stability with respect to current and temperature, and the propagation time of an error signal travelling around the loop. All of these issues are critical in achieving true phase lock.

Future research will now be directed toward utilizing better behaved laser diodes and phase modulators with serrodyne waveform generators. The eventual goal is to build an optical Costas type loop, which would then allow the practical use of coherent optical communications.

APPENDIX A

TABULATED VALUES OF THE INTEGRAL FORM

$$I_n = \frac{1}{2\pi j} \int_{-j\infty}^{j\infty} ds \, \frac{c(s)c(-s)}{d(s)d(-s)}$$

and

$$c(s) = c_{n-1}s^{n-1} + \ldots + c_0 \qquad\qquad d(s) = d_n s^n + \ldots + d_0$$

$$I_1 = \frac{c_0^2}{2d_0 d_1} \qquad\qquad\qquad I_2 = \frac{c_1^2 d_0 + c_0^2 d_2}{2d_0 d_1 d_2}$$

$$I_3 = \frac{c_2^2 d_0 d_1 + (c_1^2 - 2c_0 c_2)d_0 d_3 + c_0^2 d_2 d_3}{2d_0 d_3(-d_0 d_3 + d_1 d_2)}$$

$$I_4 = \frac{c_3^2(-d_0^2 d_3 + d_0 d_1 d_2) + (c_2^2 - 2c_1 c_3)d_0 d_1 d_4 + (c_1^2 - 2c_0 c_2)d_0 d_3 d_4 + c_0^2(-d_1 d_4^2 + d_2 d_3 d_4)}{2d_0 d_4(-d_0 d_3^2 - d_1^2 d_4 + d_1 d_2 d_3)}$$

$$I_5 = \frac{1}{2\Delta_5}\,[c_4^2 m_0 + (c_3^2 - 2c_2 c_4)m_1 + (c_2^2 - 2c_1 c_3 + 2c_0 c_4)m_2 + (c_1^2 - 2c_0 c_2)m_3 + c_0^2 m_4]$$

where

$$m_0 = \frac{1}{d_5}\,(d_3 m_1 - d_1 m_2) \quad m_1 = -d_0 d_3 + d_1 d_2 \qquad m_2 = -d_0 d_5 + d_1 d_4$$

$$m_3 = \frac{1}{d_0}\,(d_2 m_2 - d_4 m_1) \quad m_4 = \frac{1}{d_0}\,(d_2 m_3 - d_4 m_2)$$

$$\Delta_5 = d_0\,(d_1 m_4 - d_3 m_3 + d_5 m_2)$$

BIBLIOGRAPHY

1. Solo, D. M., <u>Homodyne Detection of a Biphase Modulated 1.3 μm Optical Carrier in Polarization Preserving Fiber</u>, MIT-EE, MS Thesis, 1987.

2. Gardner, F. M., <u>Phaselock Techniques</u>, Wiley-Interscience, 1966.

3. Blanchard, A., <u>Phase-Locked Loops</u>, Wiley-Interscience, 1976.

4. Ho, S., <u>Reduction of Frequency Noise in Semiconductor Lasers</u>, MIT-EE, MS Thesis, 1984.

5. Brown, R. G., <u>Introduction to Random Signal Analysis and Kalman Filtering</u>, Wiley, 1983.

6. Ohtsu, M. and Tabuchi, N., "Electrical Feedback and its Network Analysis for Linewidth Reduction of a Semiconductor Laser," submitted to <u>Journal of Lightwave Technology</u>, 1987.

7. Grant, M. A., Michie, W. C., and M. J. Fletcher, "The Performance of Optical Phase-Locked Loops in the Presence of Nonnegligible Loop Propagation Delay," <u>Journal of Lightwave Technology</u>, April, 1987, Volume LT-5, Number 4, p. 992.

8. Hecht, E. and A. Zajac, <u>Optics</u>, Addison-Wesley Publishing Company, 1979.

9. Nakano, Y., Y. Itaya, M. Fukuda, Y. Noguchi, H. Yasaka, and K. Oe, "1.55 μm Narrow-Linewidth Multielectrode DFB Laser for Coherent FSK Transmission," <u>Electronic Letters</u>, Vol. 23, No. 16, July 30, 1987, pp. 826-828.

10. Nillson, O., L. Gillner, and E. Goobar, "Formulas For Direct Frequency Modulation Response of Two-Electrode Diode Lasers: Proposals for Improvement," <u>Electronic Letters</u>, Vol. 23, No. 25, December 3, 1987, pp. 1371-1372.